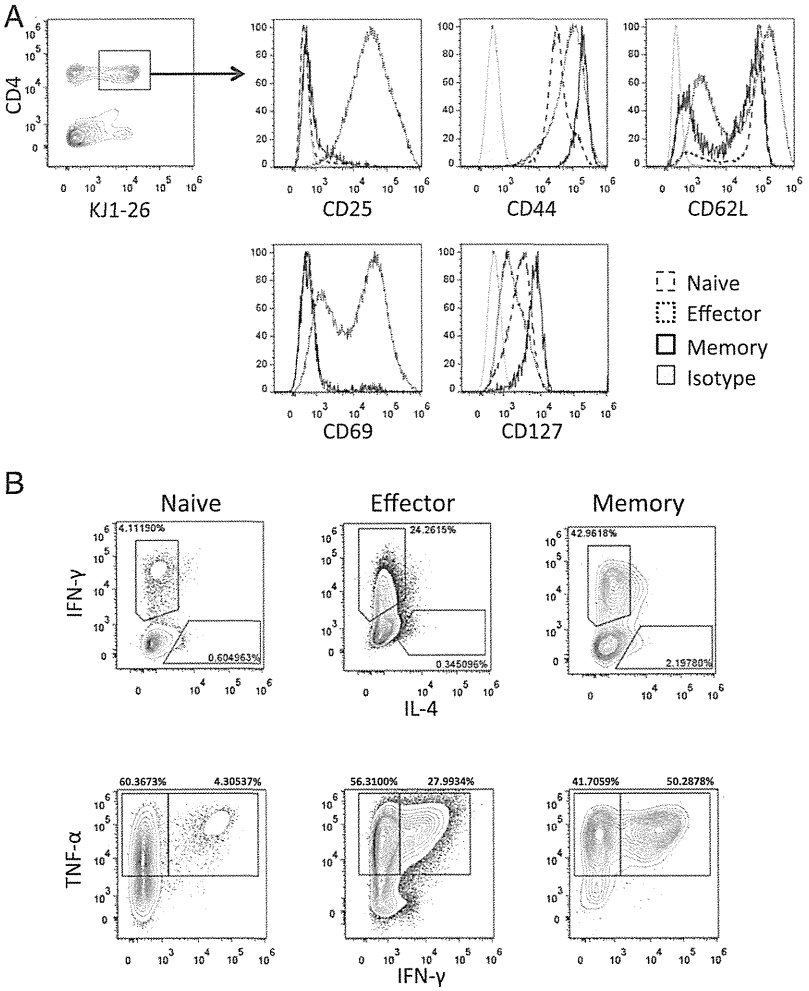

FIGURE 1. Surface marker and cytokine expression in naive and Ag-specific effector and memory CD4$^+$ T cells. Splenic CD4$^+$ T cells from DO11.10-Tg mice were stimulated with an OVA323–339 peptide plus APC for 5 d in vitro, resulting in Ag-specific effector cells, followed by transfer into normal syngeneic BALB/c recipient mice to generate memory cells. (**A**) Surface markers on CD4$^+$ T cells (double positive for KJ1 and CD4, *upper left panel*) were analyzed by flow cytometry. (**B**) IFN-γ, IL-4, and TNF-α production by naive, effector, and memory CD4 T cells was assessed by intracellular cytokine staining.

Real-time PCR

cDNA was prepared from total RNA samples using an Applied Biosystems (Foster City, CA) cDNA Archive Kit and random primers. The assay was run in triplicate for each RNA sample, in accordance with the manufacturer's recommendations, with each reaction containing 50 ng total cDNA (as total input RNA) per 20-μl reaction volume. The cycling conditions for SYBR Green dye I quantitative real-time PCR with 2× Applied Biosystems Universal Master Mix were 2 min at 50°C, 10 min at 95°C, followed by 40 rounds of 15 s at 95°C and 1 min at 60°C, with analysis by an Applied Biosystems 7500 PCR system. β-actin was used as the reference gene. Primer sequences are listed in Supplemental Table I. Data acquisition and analysis were performed using SDS 2.1 software in relative quantity mode, with each sample analyzed three times. After PCR, CT values were determined and used to calculate normalized $2^{-\Delta\Delta CT}$ values.

Luciferase reporter assay

Fragments of DMRs of the mouse *Nr1D1*, *Ptgir*, *Tnfsf4*, *Tbx21*, *Cish*, *Chsy1*, *Sdf4*, *Hps4*, *Sema4d*, *Mtss1*, *Klf7*, *Wdfy2*, *Nr5a1*, and *MapK1ip1* loci were amplified by PCR using genomic DNA as a template and the primers shown in Supplemental Table I. To generate a luciferase reporter vector on a CpG-free background, the 500–800-bp PCR product was inserted into the pCpGL-CMV/EF1 vector (a gift from Dr. M. Rehli and Dr. M. Klug) using the In-Fusion cloning system (Clontech), replacing the CMV enhancer with the DMR regions (19).

The luciferase reporter vector pCpGL-Cish-DMR/EF1 was methylated in vitro using methylase SssI (New England BioLabs), according to the manufacturer's instructions, followed by purification using a QIAquick PCR clean-up kit. In control samples using pCpGL-EF1 and pCpGL-Cish-DMR/EF1, the methyl-group donor S-adenosylmethionine was omitted. Successful methylation of the reporter plasmid containing the DMR was verified by reaction with the methylation-sensitive and methylation-resistant enzymes HpaII and MspI, respectively.

EL-4 T cells (5×10^6 cells) were transfected with 2.5 μg either methylated or unmethylated pCpGL-DMR/EF1 vector or using a control plasmid with no insert, in triplicate. Synthetic *Renilla* luciferase reporter vector (pRL-TK; Promega) was cotransfected (1.5 μg) and served as an internal control for efficiency. EL-4 cells were electroporated with a Bio-Rad Gene Pulser at 270 V and a capacitance of 975 μF. Twelve hours later, transfected cells were stimulated with PMA (50 ng/ml) and ionomycin (0.5 μg/ml) for 16 h. The cells were harvested, and luciferase activity was measured by the Dual Luciferase Assay system using an Orion L luminometer. Firefly raw light unit data were normalized to *Renilla* luciferase activity and expressed relative to the control vector with no insert.

Gene ontology

Gene ontology was estimated using GOstat software (25).

Table I. Genome-wide methylation sequencing summary for CD4$^+$ T cell DNA cut with HpaII or MspI restriction nuclease

Cell Type	Nuclease	No. of Hits in Genome	Unique Tags[a]	%
Naive	HpaII	9,902,632	5,074,880	51
	MspI	12,994,381	5,499,474	42
Effector	HpaII	9,349,718	6,039,406	65
	MspI	9,673,142	6,140,353	63
Memory	HpaII	13,582,273	7,055,612	52
	MspI	9,943,128	4,193,004	42
Total		65,445,274	34,002,729	52

Twenty-base pair MSCC tags were mapped in the genome.
[a]Number of tags in restriction sites for analysis of DNA methylation.

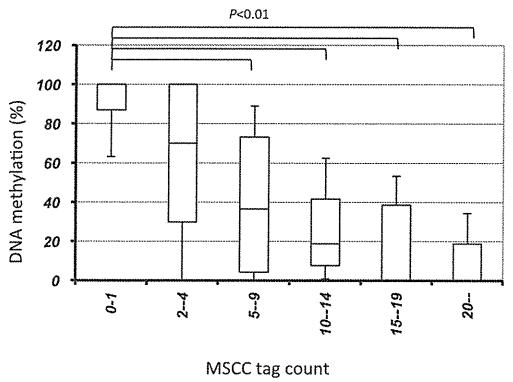

FIGURE 2. The relationship between MSCC tag counts and bisulfite sequencing data. To validate the methylation levels determined by MSCC, we designed primers targeting 130 profiled locations in bisulfite-treated DNA and performed PCR amplification and Sanger sequencing of the PCR product. Horizontal lines represent median methylation as determined by bisulfite sequencing, boxes represent the quartiles, and whiskers mark the 5th and 95th percentiles. $p < 0.01$, Kruskal–Wallis H test.

Bisulfite sequencing

Bisulfite sequencing was performed to verify SOLiD data. Bisulfite modification of genomic DNA was performed using the EpiTect Bisulfite Kit (QIAGEN). We used Methyl Primer Express software (Applied Biosystems) to design primers. Bisulfite-treated DNA was amplified by PCR. The PCR products were cloned into the pCR2.1-TOPO vector and transformed into One Shot TOP10 Competent Cells (Invitrogen). At least 24 clones were sequenced using an ABI3730 Sequencer. The data were analyzed using QUMA, a quantification tool for methylation analysis (Riken Institute of Physical and Chemical Research, Yokohama, Japan).

Statistical analysis

Comparisons of each 5′-end tag were performed using Z-test statistics (24).

Accession number

5′-end and MSCC tags have been deposited in the National Center for Biotechnology Information Sequence Read Archive (http://www.ncbi.nlm.nih.gov/sra) under accession number SRP007816.

Results

Isolation of Ag-specific memory CD4$^+$ T cells

To characterize memory T cells using methylome and transcriptome analysis, we generated memory CD4$^+$ T cells from DO11.10 OVA-specific TCR-Tg mice. Splenic CD4$^+$ T cells from the DO11.10-Tg mice were stimulated with an OVA323–339 peptide plus allophycocyanin for 5 d in vitro and then transferred i.v. into normal syngeneic BALB/c recipient mice. The transferred DO11.10-Tg T cells were monitored by staining with a clonotypic KJ1 mAb. At the time of transfer, cell surface marker expression was CD44^{high} CD127$^+$ CD25$^+$ CD69$^+$ and CD62L$^+$, but by 4 wk after cell transfer the activation markers CD25 and CD69 were no longer expressed (Fig. 1A). These observations support the development of effector and memory T cell phenotypes, respectively. To confirm the functional status of these cells, cytokine-production profiles of naive and Ag-stimulated effector and memory cell populations were investigated. Within effector and memory T cell populations, 24 and 43%, respectively, expressed IFN-γ but not IL-4, within which 28 and 50% of cells coexpressed TNF-α (Fig. 1B).

DNA-methylation profiling in memory T cells

In this study, we used a recently developed MSCC method (23) that enables high-throughput, genome-wide identification of methylated CpG sites by SOLiD sequencing. Using the HpaII restriction nuclease, which recognizes unmethylated CCGG, most short-sequence tag fragments at HpaII cleavage sites can be uniquely mapped to genome locations. Methylation-sensitive restriction enzymes typically have a recognition site that contains a CpG dinucleotide, and cleavage is blocked if that site is methylated. Sites with many reads are inferred to have low methylation levels, whereas sites with few or no reads are inferred to have high methylation levels. The murine genome contains 1,594,139 CCGG sites, of which 1,130,065 (71%) can be uniquely mapped. Although each restriction enzyme site can generate two library tags, we considered the sum of tag sequences for each restriction enzyme site. A total of 619,060 sites (55%) was located within the promoter and gene body regions of unique genes, and 11% of these were within CpG islands (CGIs). A control library was also constructed by replacing HpaII with MspI, a methylation-insensitive isoschizomer of HpaII. The tags cut with MspI were used for determining zero-tag count or nonhit sites, because no tag from a HpaII library may correspond to a fully methylated site or false negative.

Using the SOLiD platform, ~65 million reads of methylation tags from naive, effector, and memory CD4$^+$ T cell genomes cut with HpaII or MspI were aligned to the mouse genome, with at most two mismatches, to allow for sequencing errors and single nucleotide polymorphisms. Thirty-four million (52%) of these tags were aligned to unique sites after repetitive sequences were excluded (Table I). These MSCC data were analyzed for the methylation levels of individual sites based on bisulfite sequencing. When MSCC tag counts and DNA methylation for randomly selected HapII sites were compared, the number of MSCC methylation tags correlated with the methylation levels derived from bisulfite data, consistent with results reported previously (23) (Fig. 2). Therefore, we defined three categories of methylation sites: low or hypo (median methylation <20%), intermediate (>20 to <80%), and high or hyper (>80%). A total of 65 and 64% of unique CpG sites in naive and memory CD4$^+$ T cells, respectively, was hypermethylated, whereas 13% in both naive and memory cells had low methylation. Around TSSs, 28 and 31% of sites in naive and memory cells, respectively, were hypermethylated, whereas 45 and 41%, respectively, had low methylation. In addition, only 28 and 30% of CGIs in naive and memory cells, respectively, were methylated.

Comparison of CpG methylation between naive and memory T cells

To observe changes in DNA methylation during T cell differentiation, the methylation status of CpG sites in gene-associated

No. of DMRs	No. of sites	*P-value*	Position
52	96,011	3.05E-7	Promoter+1st exon
54	84,749	2.00E-04	Exon (2nd–)
446	438,300	9.03E-01	Intron
592	511,005	1.06E-05	Inter-genic regions
1144	1,130,065		Total

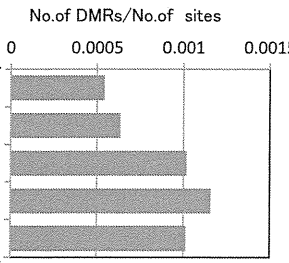

FIGURE 3. DMRs in DNA from naive and memory CD4$^+$ T cells. DMRs were classified based on their location in promoter (up to 500 bp from a TSS, based on RefSeq annotation), exon, intron, and intergenic regions based on their position relative to known genes. The number of sites represents defined HpaII restriction sites. The p values were calculated using the Fisher exact test.

Table II. Methylation of the 5′-region of naive and memory CD4$^+$ T cell genes with a DMR in an intron

No. of Tags		
Naive cells	Memory cells	No. of Genes (%)
Hypomethylation (≥10)	Hypomethylation (≥10)	273 (87.5)
Hypomethylation (≥10)	Hypermethylation (≤2)	0 (0)
Hypermethylation (≤2)	Hypomethylation (≥10)	1 (0.3)
Hypermethylation (≤2)	Hypermethylation (≤2)	29 (9.3)
Obscure methylation		9 (2.9)
Total		312 (100)

regions (the gene body including 500 bp upstream from the TSS) was compared between naive and memory T cells. When a DMR was defined as a change from 0 to >10 tags at sites cut by MspI, 1144 sites were identified as DMRs during T cell differentiation (Supplemental Table II). Fifty-one percent (552) of these DMRs were in gene-associated regions, and 467 sites associated with 437 genes were unmethylated in memory cells. In contrast, 85 sites associated with 84 genes were methylated in memory cells. The remaining 49% of the DMRs were in intergenic regions. Fig. 3 shows the DMR positions in the genome. The number of DMRs in the 5′-region (500 bp upstream from the TSS and first exon) was significantly lower than in other regions. Many DMRs were located in introns, with a few in CGIs. Our data indicated that DNA methylation in gene-promoter regions did not always correspond to a repressive epigenetic event in CD4$^+$ T cells. It is well known that the region upstream of a gene, including the promoter, is important for gene expression. Thus, we examined the DNA methylation status of gene-upstream regions (promoter and first exon) for DMRs. Others investigators reported a correlation between the methylation status of adjacent CpG sites and a high incidence of short-range comethylation (26, 27). Eighty-eight percent of genes with DMRs showed hypomethylation in their promoter/first exon in naive and memory T cells (Table II). CpG methylation of the first intron and second exon of *Cish* and of the first intron of *Tbx21*, but not of the promoter regions, was different between naive and memory T cells (Fig. 4). The results of MSCC analysis of a series of DMRs was consistent with bisulfite sequencing data. These data suggest that DNA methylation in the gene body (introns and after second exons) may be characteristic of the memory cell phenotype. To identify the function of genes differentially methylated between naive and memory T cells, genes with DMRs were classified using the Gene Ontology Consortium database (GO) (Table III). Genes associated with cell communication, signal transduction, and intracellular signaling pathways tended to be hypomethylated in memory T cells. In contrast, genes associated with development processes and biological regulation tended to be hypomethylated in naive T cells.

DNA methylation and gene expression in memory T cells

To investigate the relationship between gene expression and changes in CpG methylation in DMRs, we analyzed the gene expression of naive cells, in vitro–activated effector cells, and memory CD4$^+$ T cells using the Illumina/Solexa sequencing system. More than 12 million 25-base 5′-SAGE tags were obtained from the three libraries and matched to sequences in the

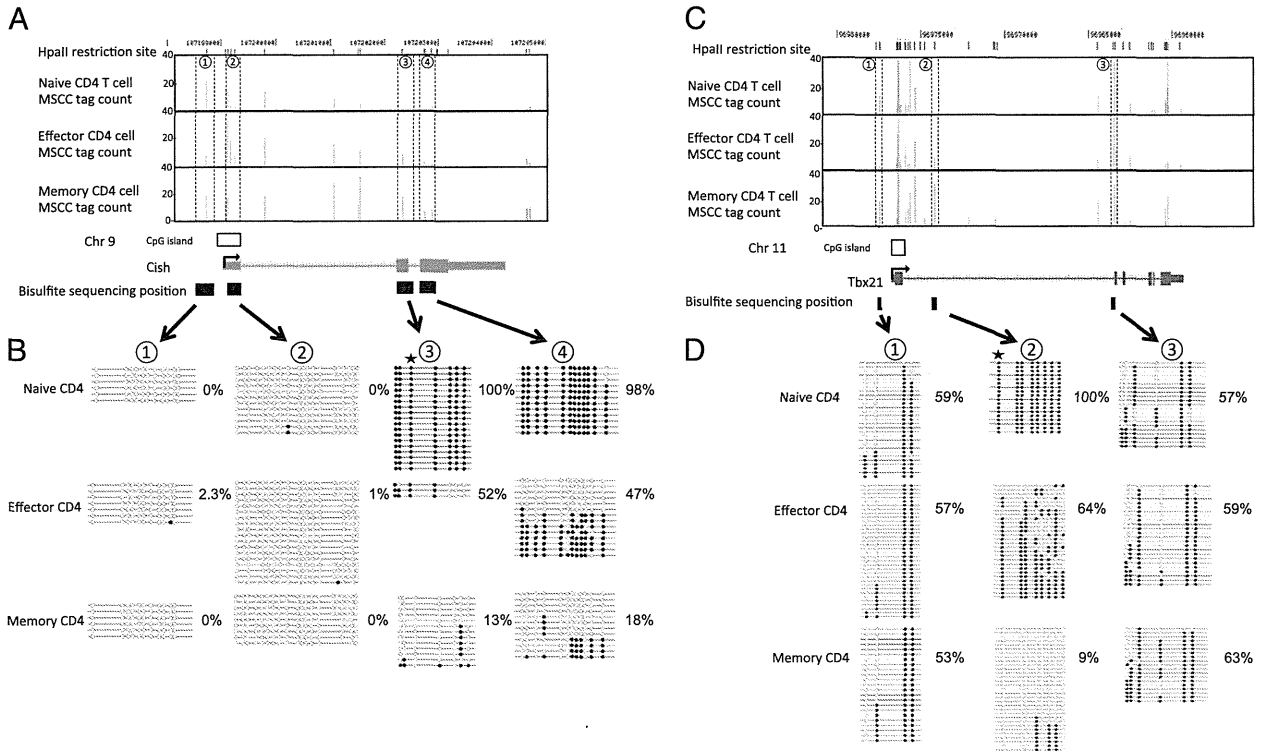

FIGURE 4. DMRs in the *Cish* and *Tbx21* loci of naive, effector, and memory T cells. Genomic organization of the mouse *Cish* (**A**) and *Tbx21* (**C**) loci, showing transcription start sites (arrows), single CGI (boxes), and exons (light blue). MSCC analysis of naive, effector, and memory T cells was across the 5′-end of each loci. Each vertical line (brown) represents a mean normalized tag from the MSCC analysis at the genomic location (listed on the *x*-axis) within the *Cish* and *Tbx21* loci on chromosomes 9 and 11, respectively (University of California, Santa Cruz genome browser). Results of genomic bisulfite sequencing for *Cish* (**B**) and *Tbx21* (**D**). Each row of circles represents an individual clone sequenced in the analysis after bisulfite treatment and PCR. Open circles indicate CpG sites at which no DNA methylation was detected. Filled circles indicate CpG sites that were methylated. Stars indicate the position of restriction sites detected by MSCC. Percentage values indicate the DNA methylation ratio of each region, as measured by bisulfite sequencing.

Table III. Gene ontology of DMR-associated genes

Best GO	Category	Count	Total	p Value[a]
Hypomethylated in memory T cells				
GO:0007154	Cell communication	119	5560	3.49E−18
GO:0007165	Signal transduction	111	5142	2.65E−17
GO:0007242	Intracellular signaling pathway	55	1965	4.94E−14
GO:0007267	Cell–cell signaling	25	640	5.25E−11
GO:0032502	Developmental process	69	3347	1.20E−08
GO:0007275	Multicellular organismal development	53	2299	1.20E−08
GO:0032501	Multicellular organismal process	75	3822	2.33E−08
GO:0048731	System development	39	1605	5.67E−07
GO:0065007	Biological regulation	109	6731	7.44E−07
GO:0050789	Regulation of biological process	101	6140	1.22E−06
GO:0007215	Glutamate signaling pathway	6	21	3.93E−06
GO:0048519	Negative regulation of biological process	30	1182	7.67E−06
GO:0048856	Anatomical structure development	43	2005	8.94E−06
GO:0009966	Regulation of signal transduction	23	800	8.94E−06
GO:0048523	Negative regulation of cellular process	29	1137	8.96E−06
Hypomethylated in memory T cells				
GO:0032502	Developmental process	19	3347	4.57E−06
GO:0065007	Biological regulation	29	6731	4.57E−06
GO:0050789	Regulation of biological process	27	6140	6.68E−06
GO:0016070	RNA metabolic process	21	4155	8.43E−06

[a]Each category was based on a p value < 1.0E−05.

murine genome (Table IV). Seventy-four percent of unique mapped tags were associated with RefSeq cDNA sequences, corresponding to ~12,000–14,000 different protein-coding genes in this cell type (Supplemental Table III). The expression level of 1256 genes was significantly different between naive and effector cells, whereas 259 genes were expressed significantly differently between naive and memory cells ($p < 0.001$, >10-fold difference). The 30 genes with the largest relative difference between effector and naive cells and between memory and naive cells are listed in Table V.

When gene-expression levels and DMRs were compared between naive and memory CD4 T cells, 24 DMRs were associated with increased expression of genes (e.g., CXCR6, Tbox21, Chsy1, and Cish) in memory cells compared with naive cells (>10 tags and >4-fold difference) (Table VI). In contrast, 27 DMRs were associated with decreased expression of other genes (e.g., Maff, Ephb6, and Trpm2). Classification using GO revealed that these genes are related to signal transduction, cell communication, and immune responses. These findings indicate that key genes relating to the memory phenotype undergo variable changes in DNA methylation during $CD4^+$ T cell differentiation.

The relationship between DNA methylation and enhancer activity

To examine the functional implications of these DMRs, we constructed a luciferase reporter vector consisting of the EF1 promoter and sequences derived from the DMR in the introns of 15 genes, which positively and negatively correlated with gene expression. Transient transfections were performed in untreated or P/I-treated EL-4 T cells using unmethylated (CpG) or in vitro SssI-methylated (mCpG) reporter plasmids. The transcriptional activity of the luciferase reporter construct containing the DMR of *Ptgir*, *Tnfsf4*, *Tbx21*, *Cish*, *Chsy1*, *IL7r*, and *Acot7* genes was 2-fold greater than that of the empty control vector (pCpGL-EF1) (Fig. 5). For these genes, transcriptional activation was reduced following in vitro methylation of the CpGs in the corresponding DMRs, demonstrating a suppressive effect of methylation on enhancer function. In contrast, for the luciferase reporter constructs containing the DMR of seven of the eight genes that showed reduced expression in memory cells compared with naive cells, transcriptional activity was unchanged relative to the empty control vector. Further validation confirmed that MSCC tag counts correlated with bisulfite-sequencing data for these genes. For example, DMRs in *Klf7* and *Mapk1ip1* had higher MSCC counts in memory cells (indicating less DNA methylation) but higher expression levels in naive cells (Fig. 6). Thus, although these DMRs may possess an alternative function, such as inhibition of silencer binding to the gene region, they do not influence enhancer activity.

DNA methylation status in T cell subsets

We next investigated DNA methylation in effector $CD4^+$ T cells. Effector $CD4^+$ T cells were isolated 5 d after Ag stimulation for gene-expression analysis. Interestingly, DMR methylation in effector cells followed different kinetics during differentiation compared with naive and memory cells. DMRs were classified into six distinct groups by DNA-methylation analysis (Table VII). Twenty-seven percent of DMRs were hypermethylated in naive and effector cells but were hypomethylated in memory cells

Table IV. Summary of $CD4^+$ T cell sequencing

Cell Type	Sequenced Tags	Unique Tags	Mapped Tags (one locus)	Tags in RefSeq	Gene No.	Gene No. (>1 copy)
$CD4^+$ naive T cells	12,088,592	7,883,186	4,122,853	3,382,975	14,064	8,715
$CD4^+$ effector T cells	8,660,468	4,547,959	4,449,231	2,790,122	12,877	8,756
$CD4^+$ memory T cells	11,442,151	6,258,543	3,916,175	3,179,174	13,384	8,138

Unique tags were aligned to a position unambiguously. Unique tags in TSSs were the number of unique tags mapped to regions within 500 bases of the representative TSSs of genes in the RefSeq database. Unique tags were categorized into three groups based on the number of mismatches in individual alignments. Effector T cells were generated from $CD4^+$ T cells from DO11.10-Tg mice stimulated with an OVA peptide plus allophycocyanin conditions for 5 d in vitro. Memory CD4 T cells were isolated from spleen and lymph node at 4 wk after cell transfer. 1 copy = 20 tags/3 million tags, because human cells are predicted to contain 300,000 mRNA molecules.

Table V. Gene-expression profile of effector and memory CD4$^+$ T cells compared with naive CD4$^+$ T cells

No. of Tags in				
Naive T Cells	Effector T Cells	Memory T Cells	RefSeq	Description
Effector > Naive				
0	54,848	4	NM_008630	Metallothionein 2
2	27,314	161	NM_139198	Placenta-specific 8
1	2,483	7	NM_011340	Serine or cysteine proteinase inhibitor clade
0	1,837	66	NM_001111099	Cyclin-dependent kinase inhibitor 1A P21
1	1,620	19	NM_145158	Elastin microfibril interfacer 2
0	1,354	5	NM_013542	Granzyme B
1	1,100	185	NM_008519	Leukotriene B4 receptor 1
5	6,117	7	NM_009375	Thyroglobulin
1	931	5	NM_133662	Immediate early response 3
1	904	1	NM_053095	IL 24
0	895	20	NM_021397	Repressor of GATA
2	1,461	17	NM_007796	CTL-associated protein 2
7	5,661	3819	NM_026820	IFN-induced transmembrane protein 1
11	7,979	94	NM_010370	Granzyme A
0	713	4	NM_001080815	Gastric inhibitory polypeptide receptor
0	543	21	NM_008147	gp49 A
1	448	9	NM_133720	Cysteinyl leukotriene receptor 2
2	879	3	NM_009150	Selenium binding protein 1
50	22,626	82	NM_011401	Solute carrier family 2 facilitated glucose
0	453	2	NM_147776	von Willebrand factor A domain–related protein
3	1,202	81	NM_011498	Basic helix-loop-helix domain containing class
2	724	0	NM_008156	GPI specific
0	348	1	NM_178241	IL-8 receptor α
63	21,938	26	NM_013602	Metallothionein 1
39	13,419	53	NM_001077508	TNF receptor superfamily
1	299	38	NM_008337	IFN γ
0	326	4	NM_001004174	Hypothetical protein LOC433470
0	325	0	NM_207279	Phosphatidylinositol-specific phospholipase C X
0	322	21	NM_013532	Leukocyte Ig-like receptor
0	319	0	NM_009137	Chemokine C-C motif ligand 22
Effector < Naive				
1517	0	159	NM_009777	Complement component 1 q subcomponent, B chain
665	0	93	NM_007574	Complement component 1 q subcomponent, C chain
590	0	39	NM_007572	Complement component 1 q subcomponent, A chain
426	0	43	NM_001083955	Hemoglobin α adult chain 2
407	0	384	NM_011703	Vasoactive intestinal peptide receptor 1
3535	10	1,617	NM_008052	Deltex 1 homolog
2037	7	121	NM_001042605	CD74 Ag isoform 1
306	0	4	NM_019577	Chemokine C-C motif ligand 24
289	0	14	NM_007995	Ficolin A
313	1	13	NM_001080934	Solute carrier family 16 monocarboxylic acid
219	0	5	NM_001037859	Colony stimulating factor 1 receptor
178	0	139	NM_033596	Cistone cluster 2 H4
146	1	14	NM_011414	Secretory leukocyte peptidase inhibitor
387	3	302	NM_013832	RAS protein activator like 1 GAP1 like
120	0	19	NM_133209	Paired immunoglobulin-like type 2 receptor β
117	0	9	NM_008220	Hemoglobin β adult major chain
96	1	33	NM_025806	Hypothetical protein LOC66857
78	0	102	NM_145227	2′-5′ oligoadenylate synthetase 2
78	0	163	NM_178185	Histone cluster 1 H2ao
78	0	283	NM_001033813	Hypothetical protein LOC619310
85	1	7	NM_008076	γ-aminobutyric acid GABA-C receptor
74	0	3	NM_177686	C-type lectin domain family 12 member a
79	1	3	NM_016704	Complement component 6
71	1	6	NM_009913	Chemokine C-C motif receptor 9
64	0	11	NM_138673	Stabilin-2
64	0	9	NM_001024932	Paired immunoglobulin-like type 2 receptor β 2
69	1	5	NM_011518	Spleen tyrosine kinase
523	9	28	NM_009525	Wingless-related MMTV integration site 5B
59	0	4	NM_009721	Na+/K+ -ATPase β 1 subunit
1615	28	734	NM_010494	ICAM 2
Memory > Naive				
7	5,661	3819	NM_026820	IFN-induced transmembrane protein 1
2	13	931	NM_001099217	Lymphocyte Ag 6 complex locus C2
15	59	3884	NM_010741	Lymphocyte Ag 6 complex locus C
1	1,100	185	NM_008519	Leukotriene B4 receptor 1
2	122	360	NM_015789	Dickkopf-like 1
1	5	163	NM_010553	IL 18 receptor accessory protein
0	309	179	NM_031395	Synaptotagmin-like 3 isoform a
1	2	146	NM_009915	Chemokine C-C motif receptor 2

(*Table continues*)

Table V. (*Continued*)

No. of Tags in				
Naive T Cells				
Effector > Naive	Effector T Cells	Memory T Cells	RefSeq	Description
12	641	1,661	NM_011313	S100 calcium binding protein A6 calcyclin
0	73	129	NM_177716	Hypothetical protein LOC239650
23	4,403	2,963	NM_030694	IFN-induced transmembrane protein 2
209	317	22,679	NM_013653	Chemokine C-C motif ligand 5
1	114	88	NM_146064	Acyl-CoA:cholesterol acyltransferase 2
1	3	84	NM_133643	EDAR ectodysplasin-A receptor–associated death
2	27,314	161	NM_139198	Placenta-specific 8
3	16	224	NM_013599	Matrix metallopeptidase 9
1	53	70	NM_030712	Chemokine C-X-C motif receptor 6
4	72	268	NM_011311	S100 calcium binding protein A4
3	140	186	NM_019507	T-box 21
4	1,051	238	NM_024253	NK cell group 7 sequence
0	1,837	66	NM_001111099	Cyclin-dependent kinase inhibitor 1A P21
1	4	59	NM_016685	Cartilage oligomeric matrix protein
12	34	815	NM_009910	Chemokine C-X-C motif receptor 3
1	0	50	NM_016958	Keratin 14
1	41	44	NM_008967	PG I receptor IP
132	729	5,823	NM_001013384	Podocan-like 1
0	31	43	NM_010177	Fas ligand TNF superfamily member 6
1	299	38	NM_008337	IFN γ
1	1	37	NM_010730	Annexin A1
1	4	36	NM_018734	Guanylate nucleotide binding protein 4
Naive > Memory				
817	114	8	NM_207231	ADP-ribosylation-like factor 12 protein
82	37	1	NM_175274	Tweety 3
306	0	4	NM_019577	Chemokine C-C motif ligand 24
75	74	0	NM_010358	Gst μ 1
61	52	1	NM_011129	Septin 4
53	63	1	NM_027406	Aldehyde dehydrogenase 1 family member l1
51	1	1	NM_029162	Zinc finger protein 509
51	0	1	NM_008694	Neutrophilic granule protein
51	1	1	NM_153510	Paired immunoglobulin-like type 2 receptor α
51	24	1	NM_007405	Adenylate cyclase 6
48	37	1	NM_011984	Homer homolog 3
148	5	3	NM_009238	SRY-box containing gene 4
46	12	1	NM_013569	Voltage-gated potassium channel subfamily H,
44	10	1	NM_026629	Hypothetical protein LOC68235
43	25	1	NM_011692	Von Hippel-Lindau binding protein 1
219	0	5	NM_001037859	Colony stimulating factor 1 receptor
115	22	3	NM_008538	Myristoylated alanine rich protein kinase C
36	22	1	NM_177758	Zinc finger and SCAN domains 20
36	0	1	NM_013612	Solute carrier family 11 proton-coupled
36	7	1	NM_009223	Stannin
72	18	2	NM_001033929	Threonine synthase-like 2
36	53	0	NM_011232	RAD1 homolog
94	18	3	NM_011639	Thyroid receptor-interacting protein 6
30	4	1	NM_133921	Ovarian zinc finger protein
30	110	1	NM_020006	CDC42 effector protein Rho GTPase binding 4
33	16	0	NM_009372	TG-interacting factor
29	1	1	NM_013667	Solute carrier family 22 member 2
28	14	1	NM_030557	Myoneurin
177	25	6	NM_001081127	A disintegrin-like and metallopeptidase
31	103	0	NM_033612	Elastase 1 pancreatic

The 30 genes with the largest relative differences between effector and naive cells and between memory and naive cells are listed. The total number of tags from naive (3,382,975), effector (2,790,122), and memory (3,179,174) cells was normalized to 3,000,000.

(pattern 1). For example, the extent of DNA methylation in the DMR of *CXCR6* was 92% in naive cells, 80% in effector cells, and 6% in memory T cells (Supplemental Fig. 1). Moreover, 43% of DMRs were hypermethylated in the naive phase, intermediately methylated in the effector phase, and hypomethylated in the memory phase (pattern 2). In *Cish*, for example, DNA methylation in the DMR in the second exon was 100% in naive cells, 52% in effector cells, and 13% in memory cells. An additional 17% of DMRs were hypermethylated in naive cells, intermediately methylated in effector cells, and hypomethylated in memory cells (pattern 3). GO classifications for each DMR methylation pattern revealed that genes in pattern 1 mostly fell into GO categories related to cell communication and signal transduction, whereas genes in pattern 3 aligned with GO categories related to negative regulation of cellular processes (Table VIII). These data indicate that the timing of methylation changes during T cell differentiation is regulated independently for each gene.

It is well known that central and effector memory T cells are distinct in their differentiation status. Therefore, we also investigated the DNA methylation status of selected DMRs in subpopulations of central and effector memory $CD4^+$ T cells from an untreated conventional BALB/c mouse. These DMRs were different across various T cell subsets, reinforcing the finding that the methylation status of T cell subsets reflects T cell differentiation (Fig. 7).

Table VI. Correlation between DNA methylation and gene expression in naive, effector, and memory CD4$^+$ T cells

Restriction Site	Chr	No. of Nucleotides from Nearest TSS	Symbol	Description	RefSeq	Position	Distance from Nearest CGI (bp)	DNA Methylation Score[a]						Gene Expression				
								Naive Cell HpaII	Naive Cell MspI	Effector Cell HpaII	Effector Cell MspI	Memory Cell HpaII	Memory Cell MspI	N4/M4 Fold	M4/N4 Fold	Naive CD4	Effector CD4	Memory CD4
123716994	Chr9	1,392	Cxcr6	Chemokine C-X-C motif receptor 6	NM_030712	Intron1	43,618	0	5	2	7	18	4	0	78	1	53	70
96974152	Chr11	2,440	Tbx21	T-box 21	NM_019507	Intron1	−1,727	0	2	8	8	30	5	0	69	3	140	186
17493213	Chr7	1,375	Ptgir	PG I receptor IP	NM_008967	Intron1	−876	0	10	5	6	11	6	0	49	1	41	44
73291652	Chr7	37,252	Chsy1	Carbohydrate chondroitin synthase 1	NM_001081163	Intron2	−37,769	0	10	8	9	48	6	0	20	16	127	326
9453075	Chr15	6,536	Il7r	IL 7 receptor precursor	NM_008372	Intron2	383,054	0	4	6	1	13	5	0	17	29	198	498
151561336	Chr4	9,094	Acot7	Acyl-CoA thioesterase 7	NM_133348	Intron1	−9,631	0	5	5	6	12	4	0	14	66	289	949
107202323	Chr9	3,304	Cish	Cytokine inducible SH2-containing protein	NM_009895	Exon_2/3	−3,446	0	1	8	9	17	5	0	10	53	5018	528
107201507	Chr9	2,488	Cish	Cytokine inducible SH2-containing protein	NM_009895	Intron1	−2,630	0	2	0	0	12	1	0	10	53	5018	528
112879061	Chr6	17,427	Srgap3	SLIT-ROBO Rho GTPase activating protein 3	NM_080448	Intron1	−117,067	0	16	10	10	20	14	0	9	5	241	46
41404992	Chr19	54,614	Pik3ap1	Phosphoinositide-3-kinase adaptor protein 1	NM_031376	Intron3	−45,447	0	4	4	2	17	4	0	5	5	14	28
41404611	Chr19	54,995	Pik3ap1	Phosphoinositide-3-kinase adaptor protein 1	NM_031376	Intron3	−45,828	0	11	9	15	11	9	0	5	5	14	28
43981837	Chr4	11,264	Glipr2	GLI pathogenesis–related 2	NM_027450	Intron3	−11,607	0	6	1	2	32	2	0	5	59	795	285
52379040	Chr2	153,059	Cacnb4	Calcium channel voltage–dependent, β 4	NM_001037099	Intron2	99,263	0	7	7	10	34	6	0	4	6	3	26
60189952	Chr2	31,367	Ly75	Lymphocyte Ag 75	NM_013825	Intron11	−31,177	0	1	4	2	12	5	0	4	12	56	47
29371127	Chr17	3,606	Cpne5	Copine V	NM_153166	Intron1	−3,256	0	10	3	11	11	8	0	4	4	37	18
44355013	Chr17	29,493	Clic5	Chloride intracellular channel 5	NM_172621	Intron1	−29,555	0	7	10	5	52	9	0	4	4	8	14
28393931	Chr2	25,081	Ralgds	Ral guanine nucleotide dissociation stimulator	NM_009058	Intron1	−4,975	0	8	13	15	10	1	0	4	8	81	32
155388145	Chr4	342	Tnfrsf4	TNF receptor superfamily	NM_011659	Intron1	20,771	0	5	21	6	22	3	0	4	394	5522	1455
79745901	Chr17	8,528	Cdc42ep3	CDC42 effector protein Rho GTPase binding 3	NM_026514	Intron1	−7,859	0	9	3	14	15	3	0	4	5	2	19
27822267	Chr2	80,063	Col5a1	Procollagen type V, α 1	NM_015734	Intron16	−80,584	0	16	3	9	11	10	0	4	4	1	12

(*Table continues*)

Table VI. (*Continued*)

Restriction Site	Chr	No. of Nucleotides from Nearest TSS	Symbol	Description	RefSeq	Position	Distance from Nearest CGI (bp)	DNA Methylation Score[a]						Gene Expression				
								Naive Cell HpaII	Naive Cell MspI	Effector Cell HpaII	Effector Cell MspI	Memory Cell HpaII	Memory Cell MspI	N4/M4 Fold	M4/N4 Fold	Naive CD4	Effector CD4	Memory CD4
41565822	Chr6	10,256	Ephb6	Eph receptor B6	NM_007680	Intron6	−10,660	0	10	7	5	10	11	12	0	207	11	17
77375561	Chr10	54,639	Trpm2	Transient receptor potential cation channel	NM_138301	Intron29	10,730	0	5	12	8	10	3	11	0	21	2	2
58854000	Chr15	59,542	Mtss1	Actin monomer-binding protein	NM_144800	Intron3	−58,831	0	4	15	6	21	3	9	0	179	60	19
79178744	Chr15	637	Maff	V-maf musculoaponeurotic fibrosarcoma oncogene	NM_010755	Intron1	−1,005	0	2	0	1	16	1	9	0	25	122	3
38564748	Chr2	5,312	Nr5a1	Nuclear receptor subfamily 5 group A, member 1	NM_139051	Intron3	−1,049	0	9	1	0	10	2	9	0	17	13	2
75013736	Chr12	4,720	Hif1a	Hypoxia inducible factor 1 α subunit	NM_010431	Intron1	−5,274	0	10	11	7	21	4	8	0	59	276	8
49653434	Chr2	10,229	2310010M24Rik	Hypothetical protein LOC71897	NM_027990	Intron1	−10,474	0	7	2	10	13	7	7	0	51	11	8
124129324	Chr5	4,974	Clip1	Restin	NM_019765	Intron1	−4,195	0	1	8	7	10	2	7	0	289	61	44
124474362	Chr5	7,905	Vps37b	Vacuolar protein sorting 37B	NM_177876	Intron1	−7,571	0	15	0	6	10	10	6	0	2537	1085	394
63517774	Chr14	61,260	Wdfy2	WD repeat and FYVE domain containing 2	NM_175546	Intron2	−61,692	0	4	35	7	25	2	6	0	30	17	5
56872366	Chr18	4,840	Lmnb1	Lamin B1	NM_010721	Intron1	−5,420	0	5	1	6	18	2	6	0	73	53	12
3378068	Chr10	179,872	Oprm1	Opioid receptor μ 1	NM_001039652	Intron3	243,866	0	7	3	14	14	6	5	0	30	3	6
5574804	Chr10	159,689	Esr1	Estrogen receptor 1 α	NM_007956	Intron3	−58,813	0	16	1	9	11	13	5	0	46	7	9
66089658	Chr17	32,361	Rab31	Rab31-like	NM_133685	Intron1	−31,962	0	3	5	4	23	5	5	0	19	27	4
54300515	Chr13	13,018	Hrh2	Histamine receptor H 2 isoform 1	NM_001010973	Intron1	−13,119	0	6	1	10	14	0	5	0	32	4	7
71926521	Chr12	21	Frmd6	FERM domain containing 6	NM_028127	Exon_1/ 14_first exon	0	0	4	8	0	14	1	4	0	38	31	9
58574849	Chr6	28,184	Abcg2	ATP-binding cassette subfamily G, member 2	NM_011920	Intron1	15,477	0	6	7	1	10	0	4	0	39	103	9
88790629	Chr12	5,768	1810035L17Rik	Hypothetical protein LOC380773	NM_026958	Intron3	−6,286	0	4	6	2	15	9	4	0	34	130	9
64135805	Chr1	32,156	Klf7	Kruppel-like factor 7 ubiquitous	NM_033563	Intron1	−32,381	0	6	4	11	17	1	4	0	108	48	27
21359913	Chr2	70,720	Gpr158	G protein–coupled receptor 158	NM_001004761	Intron2	−69,515	0	8	0	3	13	10	4	0	11	3	3
13609664	Chr8	67,921	Rasa3	RAS p21 protein activator 3	NM_009025	intron3	−67,326	0	8	5	2	14	6	4	0	570	349	157
24828918	Chr8	48,754	Zmat4	Zinc finger matrin type 4	NM_177086	intron1	−48,830	0	10	3	14	11	16	4	0	40	5	11

(*Table continues*)

Table VI. (*Continued*)

Restriction Site	Chr	No. of Nucleotides from Nearest TSS	Symbol	Description	RefSeq	Position	Distance from Nearest CGI (bp)	DNA Methylation Score[a]						Gene Expression				
								Naive Cell HpaII	Naive Cell MspI	Effector Cell HpaII	Effector Cell MspI	Memory Cell HpaII	Memory Cell MspI	N4/M4 Fold	M4/N4 Fold	Naive CD4	Effector CD4	Memory CD4
146036806	Chr7	1,142	Mapk1ip1	MAPK-interacting and spindle-stabilizing	NM_001045483	intron1	−827	0	7	3	5	11	5	4	0	233	152	66
96960335	Chr11	16,257	Tbx21	T-box 21	NM_019507	Exon_6/6_lastExon	−15,544	19	1	1	0	0	2	0	69	3	140	186
94729332	Chr1	1,070	Gpc1	Glypican 1	NM_016696	Intron1	0	16	2	0	0	0	1	0	21	11	22	227
128915487	Chr4	10,198	C77080	Hypothetical protein LOC97130	NM_001033189	Intron1	−581	12	3	1	1	0	2	0	6	3	3	15
148238956	Chr4	60,456	Casz1	Castor homolog 1 zinc finger	NM_027195	Intron2	26,131	10	17	1	16	0	7	0	4	10	13	36
120328900	Chr2	39,292	Capn3	Calpain 3 isoform a	NM_007601	Exon_21/24	60,309	15	7	2	6	0	13	22	0	61	9	3
35990963	Chr18	1,492	Cxxc5	CXXC finger 5	NM_133687	Intron1	0	28	4	9	2	0	1	13	0	12	22	1
126838794	Chr8	83,501	Galnt2	UDP-*N*-acetyl-α-D-galactosamine: polypeptide	NM_139272	Intron3	−83,718	16	5	0	2	0	1	8	0	128	55	16
63546881	Chr14	90,367	Wdfy2	WD repeat and FYVE domain containing 2	NM_175546	Intron4	−90,799	20	1	1	9	0	6	6	0	30	17	5

The category was represented using the criteria of DMRs (changing from 0 to >10 tags at the sites able to be digested by MspI between naive and memory CD4 T cells) and gene expression (memory or naive; >10 tags and >4-fold difference). Each number of gene-expression tags from naive (3,382,975), effector (2,790,122), and memory (3,179,174) cells was normalized to 3,000,000.

[a]DNA methylation score is described in *Materials and Methods*.

Gene	MCSS Tag No. Naive	MCSS Tag No. Memory	Expression Tag No. Naive	Expression Tag No. Memory
Ptgir	0	45	12	44
Tnfrsf4	0	22	394	1455
Tbx21	0	30	3	186
Cish	0	12	53	528
Chsy1	0	48	16	326
IL7r	0	13	29	498
Acot7	0	12	66	949
RASA3	0	14	570	157
Maff	0	16	25	3
Hrh2	0	14	32	7
Mtss1	0	21	179	19
Klf7	0	17	108	27
Wdfy2	0	25	30	5
Nr5a1	0	10	17	2
Mapk1ip1	0	11	122	22

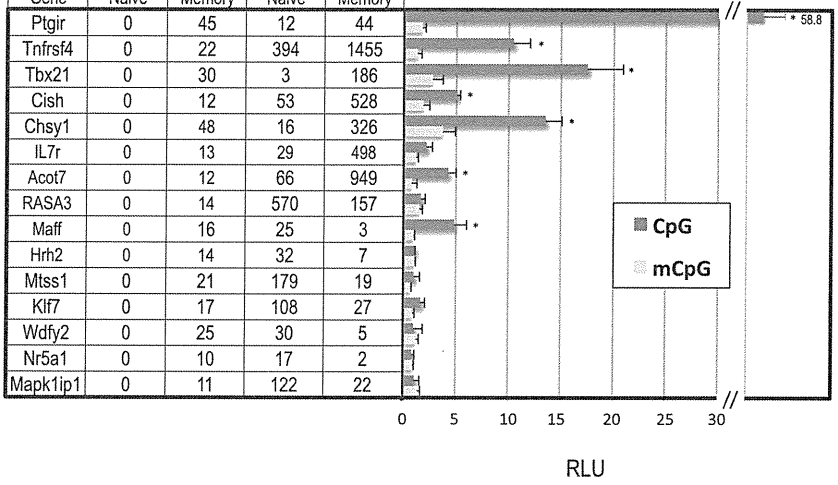

FIGURE 5. Transcriptional activity of a luciferase reporter gene in unmethylated and methylated DMR sequences from the introns of 15 genes. Transient transfections were performed with a control plasmid (pCpGL-EF1 promoter) or pCpGL-EF-DMR in P/I-treated EL-4 T cells using unmethylated (CpG) or in vitro SssI methylated (mCpG) reporter plasmids. Firefly raw light unit (RLU) data were normalized to *Renilla* luciferase activity relative to the control vector with no insert. *$p < 0.05$, unmethylated versus methylated plasmids, paired Student *t* test.

Discussion

Following activation with Ag, naive T cells differentiate into short-lived effector T cells and long-lived memory T cells. However, the molecular mechanisms behind the generation and maintenance of memory CD4$^+$ T cells remain unclear. To address this problem, we studied changes in epigenetic modification and gene expression in Ag-specific CD4$^+$ T cells using massive parallel DNA sequencing.

Phenotypically, both naive and memory T cell subsets are made up of small resting cells with upregulated IL-7R expression, which is necessary for their survival in vivo. Effector and memory T cells exhibit increased expression of adhesion markers (e.g., CD44 and LFA-1) and decreased expression of the lymph node homing receptor CD62L (28). This expression pattern was confirmed in the current study. Furthermore, our analyses indicated that, compared with naive CD4$^+$ T cells, the genes that were upregulated in memory CD4$^+$ T cells (e.g., IL-7R, Bcl2, Bcl2l1, and Cdkn1a and the chemokine-related genes CCL5, CCR2, CXCR6, and CXCR3) were related to cytokine production and development and maintenance of the memory phase. Expression of the Th1 genes IFN-γ, Tbox21, and IL18RAP also increased in memory CD4$^+$ T cells. In addition, the expression of several other genes [i.e., IFN-induced *trans*-membrane protein 1 (IFITM1) (29), Dkkl1 (30), and Il18rap (31)], which are related to proliferative capacity and Th1-type immunological reactions, increased in memory CD4$^+$ T cells compared with naive T cells.

It is well known that gene expression involves activation of transcription factors and/or epigenetic changes in the genome. CpG dinucleotides upstream of genes that are active in a particular tissue or cell type are less methylated, whereas inactive genes are surrounded by highly condensed chromatin and have densely methylated upstream CpG dinucleotides. A useful technique for gauging gene accessibility in the chromatin context is to monitor sensitivity of the relevant DNA sequences to digestion with DNaseI in intact nuclei (32). In general, genome sites encoding genes located in active chromatin that are actively transcribed or that have the potential to be transcribed upon stimulation are more sensitive to DNase I digestion than are sites encoding genes in inactive or closed chromatin. In this study, we used the recently developed MSCC method that enables cost-effective, high-throughput, genome-wide identification of methylated CpG sites. We identi-

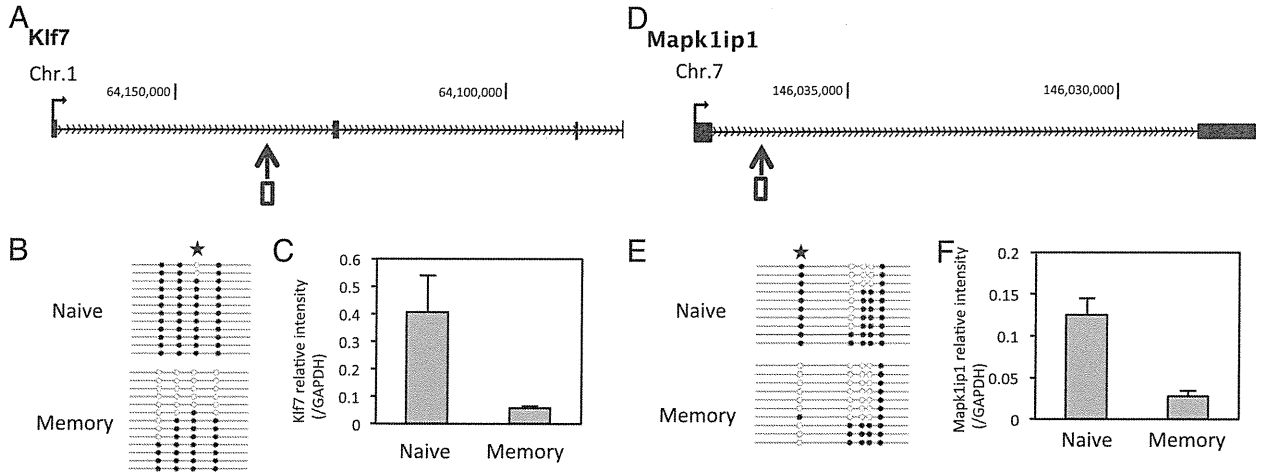

FIGURE 6. DMRs in the *Mapk1ip1* and *Klf7* loci of naive and memory T cells. Genomic organization of the mouse *Klf7* (**A**) and *Mapk1ip1* (**D**) loci showing transcription start sites (→), exons (black boxes), DMRs that were detected by MSCC (↑), and bisulfite sequencing positions (white boxes). (**B** and **E**) Results of genomic bisulfite sequencing, where each row of circles represents an individual clone sequenced following bisulfite treatment and PCR. Open circles indicate CpG sites at which no DNA methylation was detected. Stars indicate the position of restriction sites detected by MSCC. Filled circles indicate CpG sites that were methylated. (**C** and **F**) Downregulated gene expression in memory CD4 T cells measured by quantitative real-time PCR. RT-PCR was performed as described in *Materials and Methods*.

Table VII. DNA methylation status of DMRs in naive, effector, and memory $CD4^+$ T cells

Pattern	DNA Methylation Status			No. of DMR (%)
	Naive	Effector	Memory	
1	High	High	Low	314 (27%)
2	High	Int	Low	495 (43%)
3	High	Low	Low	198 (17%)
4	Low	Low	High	25 (2%)
5	Low	Int	High	42 (4%)
6	Low	High	High	70 (6%)
	Total			1144 (100%)

High, High methylation status (≤2); Int, intermediate methylation status (3–9 tags); Low, low methylation status (>9 tags).

fied 1,144 regions in the mouse genome that were differentially methylated in the process of T cell differentiation. All of these DMRs were in gene body sites without CGIs, highlighting the fact that DNA methylation can occur at sites other than CGIs. Irizarry et al. (33) reported that methylation of CGI shores that exist in close proximity (~2 kb) to CGIs is closely associated with transcriptional inactivation. Most tissue-specific DNA methylation seems not to occur within CGI, but rather at CGI shores. However, our data demonstrate that most DMRs in naive and memory $CD4^+$ T cells are not associated with CGI or CGI shores. Furthermore, most DMRs in naive and memory $CD4^+$ T cells were located in gene bodies, rather than in the promoter regions, as is the case for tumor cells.

Of the DMRs identified in naive and memory $CD4^+$ T cells, 51 were potentially associated with gene expression. Gene body methylation is common in ubiquitously expressed genes and is correlated with gene expression (23). Furthermore, intergenic methylation recently was reported to play a major role in regulating cell context–specific alternative promoters in gene bodies (34). In contrast, several groups (19, 35, 36) reported that, in human and mouse regulatory T cells, the majority of DMRs are located at promoter-distal sites and that many of these regions display DNA methylation-dependent enhancer activity in reporter gene assays. Tsuji-Takayama et al. (37) demonstrated that production of IL-10 in regulatory T cells was enhanced by IL-2 through a STAT5-responsive intron enhancer in the IL-10 locus. However, Lai et al. (38) reported that DNA methylation in an

Table VIII. GOs classified by methylation state of DMRs in effector cells

GO Hyper(N)-Hyper(E)-Hypo(M)	Genes	Count	Total	*p* Value
GO:0007154	Cell communication	25	5560	0.00507
GO:0007165	Signal transduction	23	5142	0.00772
GO:0016477	Cell migration	5	233	0.00772
GO:0006928	Cell motility	6	383	0.00772
GO:0051674	Localization of cell	6	383	0.00772
GO:0022610	Biological adhesion	9	960	0.00772
GO:0007155	Cell adhesion	9	960	0.00772
Hyper(N)-Int(E)-Hypo(M)				
GO:0007154	Cell communication	74	5560	6.09E−12
GO:0007165	Signal transduction	69	5142	2.71E−10
GO:0007242	Intracellular signal transduction	33	1965	2.85E−07
GO:0007275	Multicellular organismal development	33	2299	6.72E−05
GO:0007267	Cell–cell signaling	17	640	8.05E−05
GO:0032502	Developmental process	42	3347	0.000126
GO:0051179	Localization	51	4481	0.000243
GO:0007215	Glutamate signaling pathway	4	21	0.00075
GO:0032501	Multicellular organismal process	44	3822	0.000793
GO:0009966	Regulation of signal transduction	17	800	0.000793
GO:0048731	System development	23	1605	0.00236
GO:0051234	Establishment localization	45	4135	0.00298
GO:0006810	Transport	44	4035	0.00327
GO:0050789	Regulation of biological process	60	6140	0.00428
GO:0007268	Synaptic transmission	9	290	0.00434
GO:0048856	Anatomical structure development	26	2005	0.00472
GO:0065007	Biological regulation	64	6731	0.00472
Hyper(N)-Hypo(E)-Hypo(M)				
GO:0048523	Negative regulation of cellular process	13	1137	0.000127
GO:0048519	Negative regulation of biological process	13	1182	0.000127
GO:0050794	Regulation of cellular process	26	5704	0.000748
GO:0065007	Biological regulation	28	6731	0.00227
GO:0050789	Regulation of biological process	26	6140	0.00289
GO:0018212	Peptidyl-tyrosine modification	3	44	0.0064
GO:0007242	Intracellular signal transduction	13	1965	0.0072
GO:0007165	Signal transduction	22	5142	0.00765
GO:0007154	Cell communication	23	5560	0.00893
Hypo(N)-Int(E)-Hyper(M)				
GO:0007275	Multicellular organismal development	9	2299	0.00989
GO:0032501	Multicellular organismal process	11	3822	0.00989
Hypo(N)-Hypo(E)-Hyper(M)				
None				
Hypo(N)-Hyper(E)-Hyper(M)				
None				

GOs with a p value < 0.01 are shown.

E, Effector T cells; Hyper, hypermethylation status (more than nine tags); Hypo, hypomethylation status (two or fewer tags); Int, intermediate methylation status (three to nine tags); M, memory T cells; N, naive T cells.

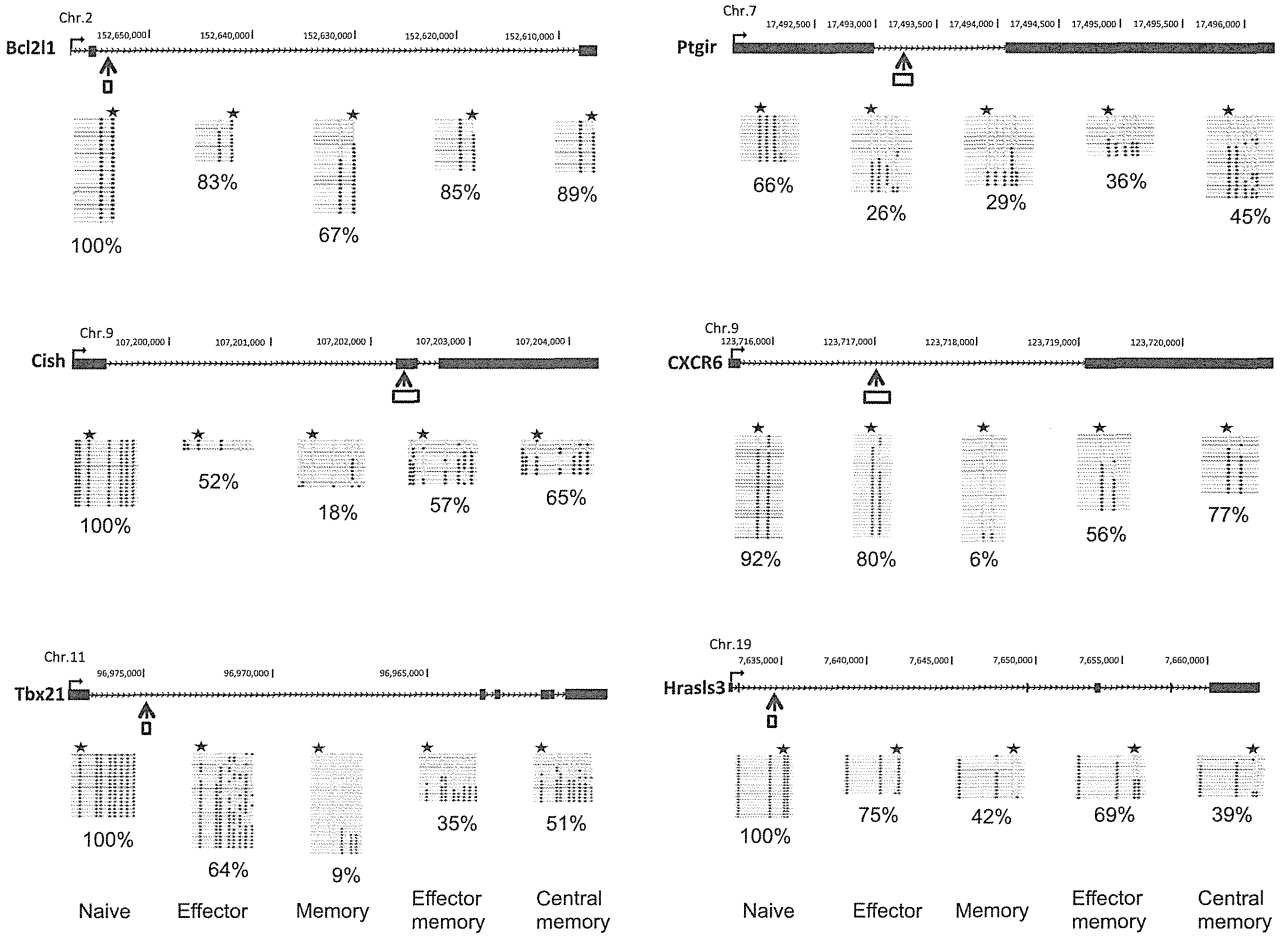

FIGURE 7. DNA methylation status of selected DMRs in subpopulations of central and effector memory $CD4^+$ T cells. $CD62L^+$ $CCR7^+$ and $CD62L^-$ $CCR7^-$ CD4 T cells from BALB/c mice were isolated to represent "central memory" and "effector memory" T cells, respectively. Genomic organization of the mouse *Cish*, *Hrasls3*, *Tbx21*, *CXCR6*, *Bcl2l1*, and *Ptgir* loci, showing transcription start sites (→), exons (black box), DMRs that were detected by MSCC (↑), and bisulfite sequencing position (white box). Graphs show results of genomic bisulfite sequencing, where each row of circles represents an individual clone sequenced in the analysis after bisulfite treatment and PCR. Open circles indicate CpG sites at which no DNA methylation was detected. Filled circles indicate CpG sites that were methylated. Stars indicate the position of restriction sites detected by MSCC. Percentage values indicate the DNA methylation ratio of each region, as measured by bisulfite sequencing.

intron can prevent enhancer-blocking transcription factor–mediated silencing. We used a reporter assay to examine the 51 gene-expression–associated DMRs and obtained results consistent with earlier reports. When loci containing DMRs were cloned into the reporter gene plasmid, the DMRs possessed enhancer activity in naive T cells in which DNA methylation was suppressed. Like previous studies, our results revealed different enhancer activities for different DMRs. It was reported that, compared with normal control cells, the DNA methylation of gene promoter regions differed in $CD4^+$ T cells in patients with rheumatoid arthritis (39), subacute cutaneous lupus erythematosus (40), and systemic lupus erythematosus (41). Together, these results suggest that, in the normal immune state, these DMRs are associated with enhancer activity rather than with promoter activity.

Genes associated with the 51 gene-expression–associated DMRs in naive and memory $CD4^+$ T cells were functionally categorized as relating to signal transduction, cell communication, and immune responses. As predicted, IL-7R, Bcl2l1, Tbox21, and CXCR6 genes were associated with changes in DNA methylation. Kim et al. (42) reported that DNA methylation is involved in regulating IL-7R expression in T cells. They found that IL-7Rα high CD8 T cells had stronger cell signaling and survival responses to IL-7 compared with IL-7Rα low CD8 T cells. Together with these findings, our results indicate that DNA methylation of the IL-7R gene in $CD4^+$ T cells may be a key mechanism for modifying IL-7–mediated T cell development and survival. In addition, in the current study, expression of Tbx21, as well as of the Th1-related gene Ptgir, was also correlated with DNA methylation. Lymph node cells from sensitized Ptgir($^{-/-}$) mice show reduced IFN-γ production and a smaller T-bet($^+$) subset compared with control mice (43).

There were also several genes relating to memory $CD4^+$ T cells homing to bone marrow (BM) that were associated with changes in DNA methylation. Tokoyada et al. (44) reported that >80% of Ly-$6C^{hi}CD44^{hi}CD62L^-$ memory CD4 T lymphocytes reside in the BM of adult mice and associate with IL-7–expressing VCAM-1 stroma cells. Our results demonstrate that Ly-6C is expressed more highly in memory $CD4^+$ T cells than in naive $CD4^+$ T cells. Because IL-7 is the main cytokine required for $CD4^+$ T cell survival (45), the BM is predicted to function as a survival niche for memory $CD4^+$ T cells. Thus, in the memory phase of immunity, memory Th cells are maintained in BM as resting, but highly reactive, cells in niches defined by IL-7–expressing stroma cells. In addition, when gene expression between $CD44^{hi}CD62L^-CD4^+$ T cells from the spleen and BM were compared, CD24, CD122, CXCR6, and CCR2 levels on $CD44^{hi}CD62L^-CD4^+$ T cells from the BM were higher than on the same cells from the spleen (45).

Our data also reveal upregulation of gene expression and unmethylation of *CXCR6* in the memory phase, suggesting that the unmethylation of DNA in gene body regions may be related to the homing of $CD44^{hi}CD62L^{-}CD4^{+}$ T cells to the BM.

In memory $CD4^{+}$ T cells, the genes Chsy1 and Itgb1 were linked to changes in DNA methylation in introns. Chsy1 synthesizes chondroitin sulfate and regulates many biological processes, including cell proliferation, recognition, and extracellular matrix deposition. Yin (46) showed that Chsy1 is the most prominent secreted protein in myeloma cell–osteoclast coculture conditioned medium and that Chsy1 activates Notch2 signaling in myeloma cells in the BM microenvironment. Therefore, Chsy1 may play an important role in cell–cell interactions, such as those between T cells and osteoclasts in the BM microenvironment. In contrast, Itgb1 is critical for maintenance of Ag-specific $CD4^{+}$ T cells in the BM (47). Therefore, DNA methylation in gene body regions is likely to play an important role in $CD4^{+}$ T cell homing to BM.

The expression of Cish was also associated with changes in DNA methylation in gene body regions. Cish is a member of the SOCS family, which was discovered as a negative regulator of cytokine signaling. However, in CD4 promoter-driven Cish-Tg mice, elevated Cish expression promotes T cell proliferation and survival after TCR activation relative to T cells in control mice (48). Moreover, Nakajima et al. (49) showed that expression of both Cish mRNA and protein is significantly increased in allergen-stimulated $CD4^{+}$ T cells from hen egg–allergic patients relative to patients not allergic to hen eggs. In addition, Khor et al. (50) identified a panel of Cish single nucleotide polymorphisms associated with increased susceptibility to infectious diseases, such as bacteremia, malaria, and tuberculosis. Thus, Cish expression caused by demethylation within the *Cish* locus in memory T cells may play a role in some infectious and allergic diseases.

In the current study, differences in methylated regions between naive and memory $CD4^{+}$ T cells did not always correlate with gene expression. The promoter and enhancer regions of differentially expressed genes were unmethylated, even in naive $CD4^{+}$ T cells. Therefore, gene expression in the naive phase is likely to be regulated primarily by the activation of transcription factors. However, changes in the DNA methylation of unsynchronized genes may prepare T cells for rapid responses following secondary stimulation via TCR signaling or other stimuli, such as inflammatory cytokines, bacteria, and viruses.

Variable DNA methylation of the enhancers of genes related to T cell development and survival represents a novel mechanism underlying the regulation of gene expression in memory $CD4^{+}$ T cells. In this study, we demonstrated the important role that methylation and demethylation of DNA in exons and introns play in regulating gene-expression patterns in Ag-specific memory $CD4^{+}$ T cells.

Acknowledgments

We thank Dr. Yong-Jun Lee and Ryu Takahashi for technical assistance and Dr. M. Klug (Department of Hematology and Oncology, University Hospital, Regensburg, Germany), for the plasmid pCpG-basic.

Disclosures

The authors have no financial conflicts of interest.

References

1. Seder, R. A., and R. Ahmed. 2003. Similarities and differences in CD4+ and CD8+ effector and memory T cell generation. *Nat. Immunol.* 4: 835–842.
2. Moulton, V. R., and D. L. Farber. 2006. Committed to memory: lineage choices for activated T cells. *Trends Immunol.* 27: 261–267.
3. Sawalha, A. H. 2008. Epigenetics and T-cell immunity. *Autoimmunity* 41: 245–252.
4. Wilson, C. B., E. Rowell, and M. Sekimata. 2009. Epigenetic control of T-helper-cell differentiation. *Nat. Rev. Immunol.* 9: 91–105.
5. Cuddapah, S., A. Barski, and K. Zhao. 2010. Epigenomics of T cell activation, differentiation, and memory. *Curr. Opin. Immunol.* 22: 341–347.
6. Portela, A., and M. Esteller. 2010. Epigenetic modifications and human disease. *Nat. Biotechnol.* 28: 1057–1068.
7. Jaenisch, R., and A. Bird. 2003. Epigenetic regulation of gene expression: how the genome integrates intrinsic and environmental signals. *Nat. Genet.* 33 (Suppl.): 245–254.
8. Bird, A. 2002. DNA methylation patterns and epigenetic memory. *Genes Dev.* 16: 6–21.
9. Jones, P. A., and D. Takai. 2001. The role of DNA methylation in mammalian epigenetics. *Science* 293: 1068–1070.
10. Li, E. 2002. Chromatin modification and epigenetic reprogramming in mammalian development. *Nat. Rev. Genet.* 3: 662–673.
11. Meehan, R. R. 2003. DNA methylation in animal development. *Semin. Cell Dev. Biol.* 14: 53–65.
12. Lee, P. P., D. R. Fitzpatrick, C. Beard, H. K. Jessup, S. Lehar, K. W. Makar, M. Pérez-Melgosa, M. T. Sweetser, M. S. Schlissel, S. Nguyen, et al. 2001. A critical role for Dnmt1 and DNA methylation in T cell development, function, and survival. *Immunity* 15: 763–774.
13. Carbone, A. M., P. Marrack, and J. W. Kappler. 1988. Demethylated CD8 gene in CD4+ T cells suggests that CD4+ cells develop from CD8+ precursors. *Science* 242: 1174–1176.
14. Wilson, C. B., K. W. Makar, and M. Pérez-Melgosa. 2002. Epigenetic regulation of T cell fate and function. *J. Infect. Dis.* 185(Suppl. 1): S37–S45.
15. Schwab, J., and H. Illges. 2001. Regulation of CD21 expression by DNA methylation and histone deacetylation. *Int. Immunol.* 13: 705–710.
16. Chen, S. C., C. Y. Lin, Y. H. Chen, H. Y. Fang, C. Y. Cheng, C. W. Chang, R. A. Chen, H. L. Tai, C. H. Lee, M. C. Chou, et al. 2006. Aberrant promoter methylation of EDNRB in lung cancer in Taiwan. *Oncol. Rep.* 15: 167–172.
17. Makar, K. W., and C. B. Wilson. 2004. DNA methylation is a nonredundant repressor of the Th2 effector program. *J. Immunol.* 173: 4402–4406.
18. Lindahl Allen, M., C. M. Koch, G. K. Clelland, I. Dunham, and M. Antoniou. 2009. DNA methylation-histone modification relationships across the desmin locus in human primary cells. *BMC Mol. Biol.* 10: 51.
19. Schmidl, C., M. Klug, T. J. Boeld, R. Andreesen, P. Hoffmann, M. Edinger, and M. Rehli. 2009. Lineage-specific DNA methylation in T cells correlates with histone methylation and enhancer activity. *Genome Res.* 19: 1165–1174.
20. Chappell, C., C. Beard, J. Altman, R. Jaenisch, and J. Jacob. 2006. DNA methylation by DNA methyltransferase 1 is critical for effector CD8 T cell expansion. *J. Immunol.* 176: 4562–4572.
21. Kersh, E. N. 2006. Impaired memory CD8 T cell development in the absence of methyl-CpG-binding domain protein 2. *J. Immunol.* 177: 3821–3826.
22. Yamashita, M., R. Shinnakasu, Y. Nigo, M. Kimura, A. Hasegawa, M. Taniguchi, and T. Nakayama. 2004. Interleukin (IL)-4-independent maintenance of histone modification of the IL-4 gene loci in memory Th2 cells. *J. Biol. Chem.* 279: 39454–39464.
23. Ball, M. P., J. B. Li, Y. Gao, J. H. Lee, E. M. LeProust, I. H. Park, B. Xie, G. Q. Daley, and G. M. Church. 2009. Targeted and genome-scale strategies reveal gene-body methylation signatures in human cells. *Nat. Biotechnol.* 27: 361–368.
24. Hashimoto, S., W. Qu, B. Ahsan, K. Ogoshi, A. Sasaki, Y. Nakatani, Y. Lee, M. Ogawa, A. Ametani, Y. Suzuki, et al. 2009. High-resolution analysis of the 5′-end transcriptome using a next generation DNA sequencer. *PLoS ONE* 4: e4108.
25. Beissbarth, T., and T. P. Speed. 2004. GOstat: find statistically overrepresented Gene Ontologies within a group of genes. *Bioinformatics* 20: 1464–1465.
26. Eckhardt, F., J. Lewin, R. Cortese, V. K. Rakyan, J. Attwood, M. Burger, J. Burton, T. V. Cox, R. Davies, T. A. Down, et al. 2006. DNA methylation profiling of human chromosomes 6, 20 and 22. *Nat. Genet.* 38: 1378–1385.
27. Irizarry, R. A., C. Ladd-Acosta, B. Carvalho, H. Wu, S. A. Brandenburg, J. A. Jeddeloh, B. Wen, and A. P. Feinberg. 2008. Comprehensive high-throughput arrays for relative methylation (CHARM). *Genome Res.* 18: 780–790.
28. Moulton, V. R., N. D. Bushar, D. B. Leeser, D. S. Patke, and D. L. Farber. 2006. Divergent generation of heterogeneous memory CD4 T cells. *J. Immunol.* 177: 869–876.
29. Yang, G., Y. Xu, X. Chen, and G. Hu. 2007. IFITM1 plays an essential role in the antiproliferative action of interferon-gamma. *Oncogene* 26: 594–603.
30. Gattinoni, L., X. S. Zhong, D. C. Palmer, Y. Ji, C. S. Hinrichs, Z. Yu, C. Wrzesinski, A. Boni, L. Cassard, L. M. Garvin, et al. 2009. Wnt signaling arrests effector T cell differentiation and generates CD8+ memory stem cells. *Nat. Med.* 15: 808–813.
31. Debets, R., J. C. Timans, T. Churakowa, S. Zurawski, R. de Waal Malefyt, K. W. Moore, J. S. Abrams, A. O'Garra, J. F. Bazan, and R. A. Kastelein. 2000. IL-18 receptors, their role in ligand binding and function: anti-IL-1RAcPL antibody, a potent antagonist of IL-18. *J. Immunol.* 165: 4950–4956.
32. Rao, A., and O. Avni. 2000. Molecular aspects of T-cell differentiation. *Br. Med. Bull.* 56: 969–984.
33. Irizarry, R. A., C. Ladd-Acosta, B. Wen, Z. Wu, C. Montano, P. Onyango, H. Cui, K. Gabo, M. Rongione, M. Webster, et al. 2009. The human colon cancer methylome shows similar hypo- and hypermethylation at conserved tissue-specific CpG island shores. *Nat. Genet.* 41: 178–186.

34. Maunakea, A. K., R. P. Nagarajan, M. Bilenky, T. J. Ballinger, C. D'Souza, S. D. Fouse, B. E. Johnson, C. Hong, C. Nielsen, Y. Zhao, et al. 2010. Conserved role of intragenic DNA methylation in regulating alternative promoters. *Nature* 466: 253–257.
35. Kim, H. P., and W. J. Leonard. 2007. CREB/ATF-dependent T cell receptor-induced FoxP3 gene expression: a role for DNA methylation. *J. Exp. Med.* 204: 1543–1551.
36. Baron, U., S. Floess, G. Wieczorek, K. Baumann, A. Grützkau, J. Dong, A. Thiel, T. J. Boeld, P. Hoffmann, M. Edinger, et al. 2007. DNA demethylation in the human FOXP3 locus discriminates regulatory T cells from activated FOXP3(+) conventional T cells. *Eur. J. Immunol.* 37: 2378–2389.
37. Tsuji-Takayama, K., M. Suzuki, M. Yamamoto, A. Harashima, A. Okochi, T. Otani, T. Inoue, A. Sugimoto, T. Toraya, M. Takeuchi, et al. 2008. The production of IL-10 by human regulatory T cells is enhanced by IL-2 through a STAT5-responsive intronic enhancer in the IL-10 locus. *J. Immunol.* 181: 3897–3905.
38. Lai, A. Y., M. Fatemi, A. Dhasarathy, C. Malone, S. E. Sobol, C. Geigerman, D. L. Jaye, D. Mav, R. Shah, L. Li, and P. A. Wade. 2010. DNA methylation prevents CTCF-mediated silencing of the oncogene BCL6 in B cell lymphomas. *J. Exp. Med.* 207: 1939–1950.
39. Janson, P. C., L. B. Linton, E. A. Bergman, P. Marits, M. Eberhardson, F. Piehl, V. Malmström, and O. Winqvist. 2011. Profiling of CD4+ T cells with epigenetic immune lineage analysis. *J. Immunol.* 186: 92–102.
40. Luo, Y., X. Zhang, M. Zhao, and Q. Lu. 2009. DNA demethylation of the perforin promoter in CD4(+) T cells from patients with subacute cutaneous lupus erythematosus. *J. Dermatol. Sci.* 56: 33–36.
41. Jeffries, M., M. Dozmorov, Y. Tang, J. T. Merrill, J. D. Wren, and A. H. Sawalha. 2011. Genome-wide DNA methylation patterns in CD4+ T cells from patients with systemic lupus erythematosus. *Epigenetics* 6: 593–601.
42. Kim, H. R., K. A. Hwang, K. C. Kim, and I. Kang. 2007. Down-regulation of IL-7Ralpha expression in human T cells via DNA methylation. *J. Immunol.* 178: 5473–5479.
43. Nakajima, S., T. Honda, D. Sakata, G. Egawa, H. Tanizaki, A. Otsuka, C. S. Moniaga, T. Watanabe, Y. Miyachi, S. Narumiya, and K. Kabashima. 2010. Prostaglandin I2-IP signaling promotes Th1 differentiation in a mouse model of contact hypersensitivity. *J. Immunol.* 184: 5595–5603.
44. Tokoyoda, K., S. Zehentmeier, A. N. Hegazy, I. Albrecht, J. R. Grün, M. Löhning, and A. Radbruch. 2009. Professional memory CD4+ T lymphocytes preferentially reside and rest in the bone marrow. *Immunity* 30: 721–730.
45. Chetoui, N., M. Boisvert, S. Gendron, and F. Aoudjit. 2010. Interleukin-7 promotes the survival of human CD4+ effector/memory T cells by up-regulating Bcl-2 proteins and activating the JAK/STAT signalling pathway. *Immunology* 130: 418–426.
46. Yin, L. 2005. Chondroitin synthase 1 is a key molecule in myeloma cell-osteoclast interactions. *J. Biol. Chem.* 280: 15666–15672.
47. DeNucci, C. C., and Y. Shimizu. 2011. β1 integrin is critical for the maintenance of antigen-specific CD4 T cells in the bone marrow but not long-term immunological memory. *J. Immunol.* 186: 4019–4026.
48. Li, S., S. Chen, X. Xu, A. Sundstedt, K. M. Paulsson, P. Anderson, S. Karlsson, H. O. Sjögren, and P. Wang. 2000. Cytokine-induced Src homology 2 protein (CIS) promotes T cell receptor-mediated proliferation and prolongs survival of activated T cells. *J. Exp. Med.* 191: 985–994.
49. Nakajima, Y., I. Tsuge, Y. Kondo, R. Komatsubara, N. Hirata, M. Kakami, M. Kato, H. Kurahashi, A. Urisu, and Y. Asano. 2008. Up-regulated cytokine-inducible SH2-containing protein expression in allergen-stimulated T cells from hen's egg-allergic patients. *Clin. Exp. Allergy* 38: 1499–1506.
50. Khor, C. C., F. O. Vannberg, S. J. Chapman, H. Guo, S. H. Wong, A. J. Walley, D. Vukcevic, A. Rautanen, T. C. Mills, K. C. Chang, et al. 2010. CISH and susceptibility to infectious diseases. *N. Engl. J. Med.* 362: 2092–2101.

European Journal of Pharmacology 724 (2014) 161–167

Contents lists available at ScienceDirect

European Journal of Pharmacology

journal homepage: www.elsevier.com/locate/ejphar

Pulmonary, gastrointestinal and urogenital pharmacology

Ursodeoxycholic acid inhibits overexpression of P-glycoprotein induced by doxorubicin in HepG2 cells

Yuki Komori [a], Sakiko Arisawa [a], Miho Takai [a], Kunihiro Yokoyama [a], Minako Honda [a], Kazuhiko Hayashi [b], Masatoshi Ishigami [b], Yoshiaki Katano [b], Hidemi Goto [b], Jun Ueyama [a], Tetsuya Ishikawa [a], Shinya Wakusawa [a,*]

[a] Division of Medical Laboratory Sciences, Department of Radiological and Medical Laboratory Sciences, Nagoya University Graduate School of Medicine, 1-1-20 Daiko-minami, Higashi-ku, Nagoya 461-8673, Japan
[b] Division of Gastroenterology, Department of Internal Medicine, Nagoya University Graduate School of Medicine, 65 Tsurumai-cho, Showa-ku, Nagoya 466-8550, Japan

ARTICLE INFO

Article history:
Received 8 October 2013
Received in revised form
12 December 2013
Accepted 12 December 2013
Available online 24 December 2013

Chemical compounds studied in this article:
Ursodeoxycholic acid (PubChem CID: 31401)
Chenodeoxycholic acid (PubChem CID: 10133)
Deoxycholic acid (PubChem CID: 222528)
Lithocholic acid (PubChem CID: 9903)
Doxorubicin (PubChem CID: 31703)
Rhodamine 123 (PubChem CID: 65217)

Keywords:
Bile acids
P-Glycoprotein
Reactive oxygen species
MDR1
Ursodeoxycholic acid

ABSTRACT

The hepatoprotective action of ursodeoxycholic acid (UDCA) was previously suggested to be partially dependent on its antioxidative effect. Doxorubicin (DOX) and reactive oxygen species have also been implicated in the overexpression of P-glycoprotein (P-gp), which is encoded by the MDR1 gene and causes antitumor multidrug resistance. In the present study, we assessed the effects of UDCA on the expression of MDR1 mRNA, P-gp, and intracellular reactive oxygen species levels in DOX-treated HepG2 cells and compared them to those of other bile acids. DOX-induced increases in reactive oxygen species levels and the expression of MDR1 mRNA were inhibited by N-acetylcysteine, an antioxidant, and the DOX-induced increase in reactive oxygen species levels and DOX-induced overexpression of MDR1 mRNA and P-gp were inhibited by UDCA. Cells treated with UDCA showed improved rhodamine 123 uptake, which was decreased in cells treated with DOX alone. Moreover, cells exposed to DOX for 24 h combined with UDCA accumulated more DOX than that of cells treated with DOX alone. Thus, UDCA may have inhibited the overexpression of P-gp by suppressing DOX-induced reactive oxygen species production. Chenodeoxycholic acid (CDCA) also exhibited these effects, whereas deoxycholic acid and litocholic acid were ineffective. In conclusion, UDCA and CDCA had an inhibitory effect on the induction of P-gp expression and reactive oxygen species by DOX in HepG2 cells. The administration of UDCA may be beneficial due to its ability to prevent the overexpression of reactive oxygen species and acquisition of multidrug resistance in hepatocellular carcinoma cells.

© 2013 Elsevier B.V. All rights reserved.

1. Introduction

Ursodeoxycholic acid (UDCA) is a tertiary bile acid in humans, and large doses have been used as a hepatoprotective drug in the treatment of antivirus therapy non-responsive chronic hepatitis C (Omata et al., 2007) and primary biliary cirrhosis (Corpechot et al., 2000). Although the detailed mechanism of its hepatoprotective effect remains to be clarified, it may be due to its antioxidative effect and protection against apoptosis caused by mitochondria injury (Mitsuyoshi et al., 1999; Rajesh et al., 2005; Okada et al., 2008; Kawata et al., 2010). As a molecular mechanism for its antioxidative effect, we recently demonstrated that UDCA induced glutathione (GSH) synthesis due to the translocation of Nrf2 into the nucleus following activation of the PI3K/Akt pathway (Arisawa et al., 2009), which may also contribute to the protection of mitochondria.

P-Glycoprotein (P-gp), a membrane drug transporter encoded by the MDR1 gene, is frequently overexpressed in tumor cells treated with chemotherapeutic agents including anthracyclines such as doxorubicin (DOX) and causes antitumor multidrug resistance (Hu et al., 1995). The physiological expression of P-gp has also been reported in various epithelial cells and it has been shown to play a role in the regulation of absorption or excretion of small amphipathic chemical compounds in organs such as the kidneys and liver (Borst and Elferink, 2002). Overexpression of the MDR1 gene was previously shown to be induced by reactive oxygen species in primary cultures of rat hepatocytes (Ziemann et al., 1999), while DOX is known to increase intracellular reactive oxygen species levels in several cells (Myers et al., 1977; Bates and

* Corresponding author. Tel./fax: +81 52 719 1558.
E-mail address: wakusawa@met.nagoya-u.ac.jp (S. Wakusawa).

0014-2999/$ - see front matter © 2013 Elsevier B.V. All rights reserved.
http://dx.doi.org/10.1016/j.ejphar.2013.12.023

Winterbourn, 1982; Ortiz et al., 2008) and decrease GSH levels in rat hepatoma cells (Ortiz et al., 2008). Hepatocellular carcinoma is the third leading cause of cancer-related death in the world (Jemal et al., 2011). Hepatitis C is a major risk factor for hepatocellular carcinoma, and DOX is frequently used as a chemotherapeutic agent in the case of transarterial chemoembolism for this disease (Tinkle and Haas-Kogan, 2012).

DOX was previously suggested to induce reactive oxygen species and P-gp; therefore, reactive oxygen species has been associated with the induction of P-gp in DOX-treated cells. In addition, because UDCA exhibits antioxidative effects, it may down-regulate the overexpression of P-gp and suppress the induction of multidrug resistance by DOX. However, the effect of UDCA on the expression or/and function of P-gp in DOX-treated hepatoma cells has not yet been examined. In this study, to evaluate the efficacy of UDCA on DOX-induced elevations in P-gp and reactive oxygen species levels, we firstly examined the effect of N-acetylcysteine (NAC), an antioxidant, on DOX-induced elevations in P-gp levels and then investigated the effects of UDCA on human hepatoma HepG2 cells. In addition, we also investigated the effects of chenodeoxycholic acid (CDCA), deoxycholic acid (DCA), and litocholic acid (LCA) to compare the effects of UDCA with those of other bile acids.

2. Materials and methods

2.1. Chemicals

UDCA was kindly supplied by Tanabe-Mitsubishi Pharmaceuticals (Osaka, Japan). CDCA, DCA, LCA, DOX, 6-carboxy-2′, 7′-1 dichlorodihydrofluorescein (CDCFH), NAC, and rhodamine 123 (Rho123) were purchased from Sigma Japan (Tokyo, Japan).

2.2. Cell culture

Human hepatoma HepG2 cells were cultured in Dulbecco's modified Eagle's medium (Sigma, Japan) supplemented with 5% (v/v) heat-inactivated fetal calf serum (BioWest, Nauille, France), 100 U/ml of penicillin (Invitrogen Japan, Tokyo, Japan), 100 μg/ml of streptomycin (Invitrogen Japan), and 0.25 mg/ml of amphotericin B (Invitrogen Japan) in 35-mm plastic dishes in the presence of 5% CO_2 at 37 °C until semi-confluency. Varying concentrations of agents were then added to the culture medium, and cells were cultured for the designated periods. Bile acids were initially dissolved in dimethylsulfoxide (DMSO, Sigma Japan) at an appropriate concentration and were then added to the culture medium. The concentration of DMSO was adjusted to 0.1% (v/v) of the culture medium in each group.

2.3. Determination of intracellular reactive oxygen species

Reactive oxygen species levels were quantified in cells using CDCFH (10 μM) as described previously (Arisawa et al., 2009). The fluorescence of CDCF was measured at 480 nm/538 nm (emission/excitation). The results were obtained as the content (nmol) per mg protein and expressed as the percentage of fluorescence compared with the control.

2.4. Determination of intracellular accumulation of DOX and Rho123

HepG2 cells were pre-incubated with or without 100 μM bile acids for 60 min, and cells were then incubated with or without 3 μM DOX in the presence or absence of 100 μM bile acids for 24 h. After the treatment, a portion of these cells were used to determine DOX, and the remaining cells were cultivated in fresh medium for 24 h. The latter cells were incubated with 3 μM Rho123 for 30 min at 37 °C. These cells were subsequently washed with phosphate-buffered saline (PBS, pH 7.4), and intracellular DOX and Rho123 were extracted with 1 ml of ethanol. A portion of these cells was used to measure fluorescence intensity with Arvo 1420 (PerkinElmer, Waltham, MA) at 480 nm/535 nm (emission/excitation) for DOX and 480 nm/580 nm (emission/excitation) for Rho123. A stock solution (3 mM) of Rho123 was prepared by dissolving it in DMSO.

2.5. Polymerase chain reaction (PCR) assay of MDR1 mRNA

We determined MDR1 mRNA levels by semi-quantitative RT-PCR. After cells were treated, total RNA was isolated using TRIzol Reagent (Invitrogen Japan) according to the manufacturer's instructions. cDNA was then prepared by incubating 0.5–1.0 μg of RNA with random primers (12.5 ng, Invitrogen Japan), RNase inhibitor (RNaseOUT, 20 units, Invitrogen Japan), 0.5 mM deoxynucleotide (dNTPs, Promega, Madison, WI), and 100 units of RNA reverse transcriptase (ReverTra Ace, TOYOBO, Tokyo, Japan) in 20 μl of the reaction buffer according to the ReverTra Ace data sheet. Following inactivation of the enzyme by incubation at 99 °C for 5 min, semi-quantitative PCR was performed with Blend Taq DNA polymerase (TOYOBO) using Thermal Cycler PxE (Thermo Fisher Scientific, Waltham, MA). PCR primers for MDR1 and GAPDH were synthesized by Hokkaido System Science. A primer set of the MDR1 gene was as follows; forward: 5′–AAGCTTAGTACCAAAGAGGCTCTG-3′, reverse: 5′–GGCTAGAAAACAATAGTGAAAACAA-3′. A primer set of GAPDH gene was as follows; forward: 5′–ACCACAGTCCATGCCATCAC-3′, reverse: 5′–TCCACCACCCTGTTGCTGTA-3′. PCR products (10 μl) were electrophoresed on a 1.5% agarose gel and visualized with ultraviolet light after immersion in an ethidium bromide solution (1 μg/ml, Sigma Japan) for 15 min. Images were taken with the digital camera CoolPix 9500 (Nikon, Tokyo, Japan) equipped with a BPB-60 filter (Fujifilm Japan, Tokyo, Japan). Densitometric analysis was performed using Image J for Windows supplied by the National Institutes of Health (Bethesda, MD).

2.6. Western blotting of P-gp

Cells were solubilized in loading dye containing 125 mM Tris (pH6.8, Sigma Japan), 5% sodium dodecylsulfate (SDS, Sigma Japan), 40% urea (Sigma Japan), and 0.2 M dithiothreitol (Sigma Japan). Samples were isolated using SDS-polyacrylamide gel electrophoresis (10% gel) and transferred onto a Hybond ECL Nitrocellulose membrane (GE Healthcare Japan, Tokyo, Japan). After blocking with skim milk, the membrane was treated with primary antibodies as follows. P-gp was detected with the C219 anti-MDR1 P-gp mouse monoclonal antibody (GeneTex, Irvine, CA) as a primary antibody and horseradish-labeled goat anti-mouse IgG2a antibody (Santa Cruz Biotechnology, Santa Cruz, CA) as a secondary antibody. The specific immunoreactive band of P-gp was detected using Immobilon Western Chemiluminescent HRP (Merck Japan, Tokyo, Japan) and a luminescence imager (Light-Capture II, ATTO, Tokyo, Japan). Densitometric analysis was performed using Image J. GAPDH (Sigma Japan) was also detected as an internal standard protein using the anti-GAPDH antibody (Sigma Japan).

Cellular protein concentrations were determined using a DC protein assay kit (Bio-Rad Laboratories, Hercules, CA).

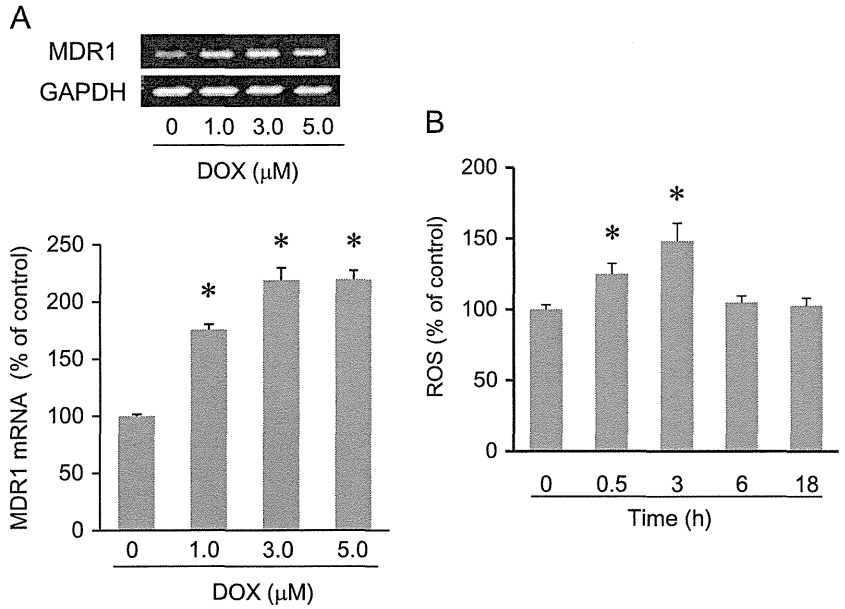

Fig. 1. Elevation in MDR1 gene expression and reactive oxygen species levels by DOX in HepG2 cells. (A) Cells were exposed to 1, 3, and 5 μM DOX or vehicle for 24 h, and RT-PCR was then conducted. Upper photographs are typical of agarose gel electrophoresis of RT-PCR products. Column graph data represent the relative expression level of MDR1 mRNA against GAPDH. (B) Cells were exposed to 3 μM DOX for the indicated periods and intracellular reactive oxygen species levels was determined as described in the Materials and Methods. Column graph data are expressed as the mean ± S.D. ($n=3$). *$P < 0.05$, significantly different from the control.

2.7. Statistical analysis

Data are expressed as the mean ± S.D. Significance was determined by a one-way analysis of variance (ANOVA) and Holm's multiple-comparison test. $P < 0.05$ was considered significant. All statistical analyses were performed using R Commander Plug-in for the EZR (Easy *R*) Package (RcmdrPlugin.EZR) (Kanda 2013).

3. Results

3.1. Increase in intracellular levels of MDR1 mRNA and reactive oxygen species by DOX in HepG2 cells and inhibition by NAC

The properties of DOX for the induction of MDR1 mRNA and reactive oxygen species levels in HepG2 cells were shown in Fig. 1A. MDR1 mRNA was induced in a dose-dependent manner after exposure to DOX for 24 h. However, our preliminary experiments indicated that this induction was not observed when cells were exposed to 3 μM DOX for 6 h (data not shown). When cells were continuously exposed to DOX (3 μM), intracellular reactive oxygen species levels increased in the early period, but returned to control levels within 6 h (Fig. 1B). To ascertain whether the elevation in MDR1 mRNA levels induced by DOX was dependent on the increase in reactive oxygen species levels, we examined the effect of NAC, an antioxidant and radical scavenger (Cotter et al., 2007). As shown in Fig. 2, the inductive effects of DOX (3 μM) on MDR1 mRNA and reactive oxygen species levels were significantly suppressed by NAC (0.5 mM). These results indicated that the induction of MDR1 mRNA by DOX depended on an elevation in intracellular reactive oxygen species levels in HepG2 cells treated with DOX.

3.2. Inhibitory effect of UDCA on DOX-induced elevations in MDR1 mRNA, P-gp, and reactive oxygen species levels in HepG2 cells

To investigate the inhibitory effect of UDCA on the DOX-induced overexpression of MDR1 mRNA and P-gp in HepG2 cells, cells were treated with 100 μM UDCA, a concentration that was shown to have anti-oxidative effects in our (Arisawa et al., 2009) and other previous studies (Mitsuyoshi et al., 1999; Rajesh et al., 2005; Okada et al., 2008).

DOX (3 μM) increased the expression of P-gp, as previously reported by Hu et al. (1995), and MDR1 mRNA in HepG2 cells. Although UDCA inhibited the DOX-induced elevation in MDR1 mRNA and P-gp levels, this dosage of UDCA itself did not influence the constitutive expression of MDR1 mRNA or P-gp (Fig. 3A–C). These results clearly demonstrated that UDCA inhibited the induction of P-gp and MDR1 gene expression by DOX in HepG2 cells.

We then investigated its effects on DOX-induced reactive oxygen species levels. As shown in Fig. 3D, UDCA inhibited the DOX-induced elevation in reactive oxygen species levels. A slight increase in reactive oxygen species levels was observed by UDCA alone.

3.3. Effects of UDCA on the intracellular accumulation of DOX and Rho123

To evaluate the transport function of DOX-induced *P*-gp and the effects of UDCA on this function, we examined the intracellular accumulation of DOX in HepG2 cells after combined exposure. As shown in Fig. 4A, UDCA increased the intracellular concentration of DOX after exposure for 24 h, while the combined exposure for 1 h failed to influence the intracellular accumulation of DOX. These results suggested that UDCA may have indirectly increased the accumulation of DOX after 24 h of exposure by inhibiting P-gp overexpression in the plasma membrane, as seen in Fig. 3A and C.

To functionally evaluate the effect of UDCA on P-gp levels, we investigated the intracellular accumulation of Rho123 after the treatment with DOX and UDCA for 24 h. As shown in Fig. 4B, UDCA by itself did not influence the uptake of Rho123. Rho123 levels were significant lower in cells pretreated with DOX than in untreated control cells. On the other hand, the accumulation of Rho123 was higher in cells pre-treated with both UDCA and DOX than in cells pre-treated with DOX alone.

These results suggested that UDCA inhibited the DOX-induced up-regulation of P-gp, which subsequently increased the intracellular accumulation of DOX and recovery of the accumulation of Rho123.

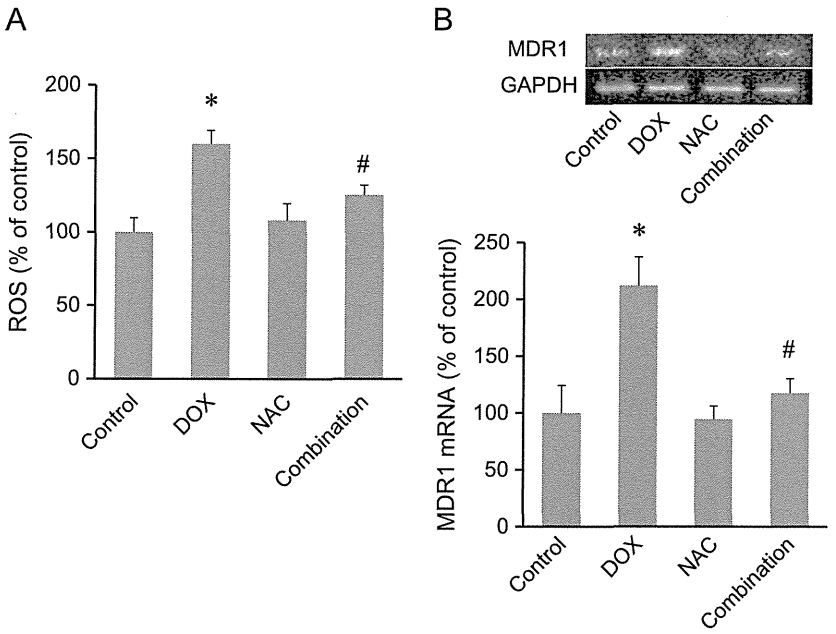

Fig. 2. Inhibition of DOX-induced increases in reactive oxygen species and MDR1 gene expression by NAC. Cells were pre-treated with 0.5 mM NAC for 1 h and then exposed to 3 μM DOX in the presence of NAC for 24 h. Reactive oxygen species measurements (A) and RT-PCR (B) were then conducted. Intracellular reactive oxygen species levels were determined using the fluorogenic dye CDCFH. Upper photographs are typical of agarose gel electrophoresis of RT-PCR products. Column graph data represent the relative expression levels of MDR1 mRNA against GAPDH. Column graph data are expressed as the mean ± S.D. ($n=3$). $^{*}P<0.05$, significantly different from the control. $^{\#}P<0.05$, significantly different from the DOX group.

3.4. Effects of CDCA, DCA, and LCA on P-gp, Rho123, and reactive oxygen species levels

We examined the effects of CDCA, DCA, and LCA to investigate if other bile acids also possessed properties similar to UDCA. As shown in Fig. 5A, CDCA (100 μM) partially inhibited the DOX-induced elevation in P-gp levels, while CDCA by itself did not affect P-gp levels. CDCA clearly inhibited the DOX-induced increase in reactive oxygen species levels (Fig. 7A), and also significantly reversed the DOX-induced reduction in intracellular Rho123 (Fig. 6A).

DCA (100 μM) did not affect DOX-induced P-gp overexpression (Fig. 5B), and had no effect on the intracellular accumulation of Rho123 (Fig. 6B) or DOX-induced elevation in intracellular reactive oxygen species levels (Fig. 7B).

The effect of LCA was investigated at 30 μM because 100 μM of LCA was cytocidal to HepG2 cells. As shown in Fig. 5C, LCA itself did not influence P-gp levels and did not influence the effect of DOX. LCA also had no effect on Rho123 uptake in cells treated without or with DOX (Fig. 6C). Although LCA increased reactive oxygen species levels by itself, it did not affect reactive oxygen species levels in combination with DOX (Fig. 7C). The reason for the lack of a correlation between LCA-induced reactive oxygen species and P-gp levels has yet to be established.

CDCA, DCA, and LCA reportedly stimulate PXR (Dussault et al., 2003) and MDR1 gene expression was previously shown to be stimulated by PXR (Geick et al., 2001). In the present study, the concentration of these bile acids may have been insufficient to induce an effect on HepG2 cells.

4. Discussion

In the natural course of chronic hepatitis C, most cases progress to liver cirrhosis, complicated by hepatocellular carcinoma. The oral administration of UDCA (typically 600 mg/day) is an alternative therapy for chronic hepatitis C in interferon-intolerant patients or non-responders, and long-term treatment is expected to improve prognosis (Omata et al., 2007). DOX is frequently used as a chemotherapeutic agent in the case of transarterial chemoembolism for hepatocellular carcinoma (Tinkle and Haas-Kogan, 2012). However, it has been shown to induce the overexpression of P-gp and antitumor multidrug resistance.

In this study, we ascertained that DOX induced P-gp, accompanied by an increase in intracellular reactive oxygen species levels, and showed that UDCA inhibited the DOX-induced up-regulation of P-gp, which reversed the decreased uptake of Rho123 in HepG2 cells pre-exposed to DOX, whereas UDCA itself had no effect on P-gp levels or Rho123 uptake. Additionally, we examined the combined effects of DOX and UDCA on P-gp levels even in Hep3B human hepatoma cells, and demonstrated that UDCA prevented the DOX-induced overexpression of P-gp (data not shown). Based on these results, it was suggested that UDCA may prevent the overexpression of P-gp induced by DOX and other anthracyclines and may also suppress the acquisition of antitumor multidrug resistance in various hepatoma cells including primary hepatoma cells. Furthermore, the clinical application of UDCA to chemotherapy for hepatocellular carcinoma, e.g. pre-and co-administration with DOX in the case of transarterial chemoembolism, may prevent the induction of P-gp by DOX and efflux of DOX from carcinoma cells, resulting in increases in its therapeutic effect.

To date, UDCA has been shown to increase MDR1 mRNA levels in Caco-2 cells, but not in intestinal or LS174T cells (Becquemont et al., 2006). On the other hand, CDCA (100 μM) increased MDR1 mRNA levels in Madin Darby canine kidney cells (Kneuer et al., 2007). In this study, UDCA and CDCA did not affect the basal expression of P-gp in HepG2 cells, but antagonized the DOX-induced increase in P-gp expression. These results indicate that the effect of UDCA and CDCA on basal MDR1 gene expression may be dependent on the types of cells and tissues studied, and these bile acids may not influence the basal expression of the MDR1 gene in hepatocellular carcinoma cells.

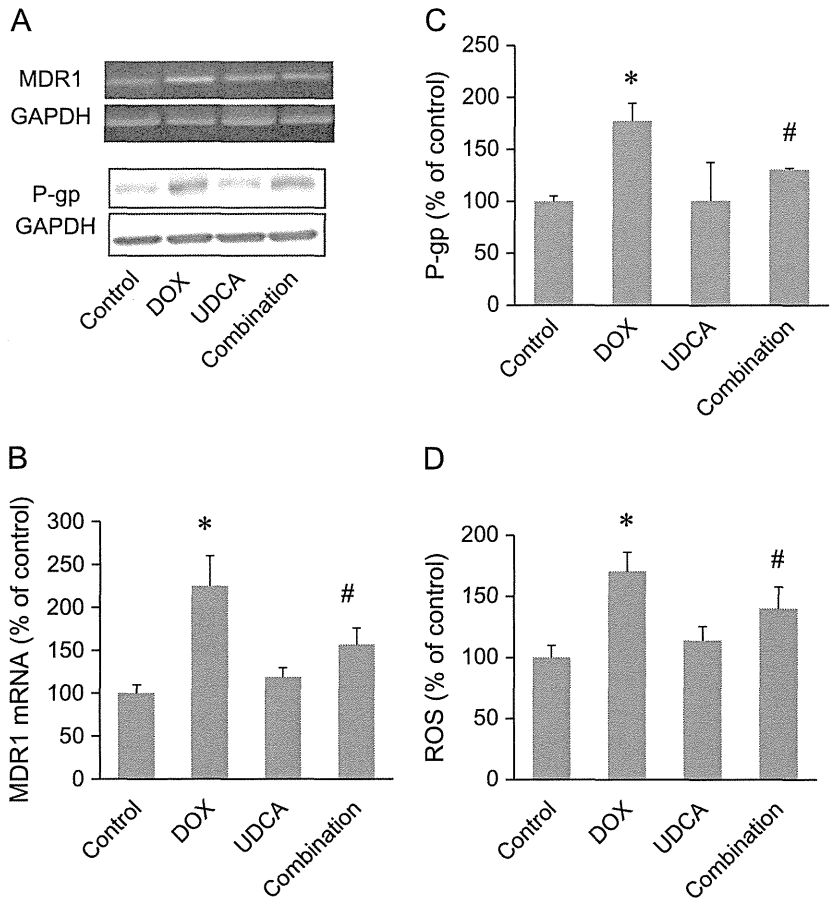

Fig. 3. Inhibitory effects of UDCA on the DOX-induced elevation in MDR1 mRNA, P-gp, and reactive oxygen species levels in HepG2 cells. HepG2 cells were pre-incubated with or without 100 μM UDCA, and were then cultivated with 3 μM DOX in the presence or absence of 100 μM UDCA for 24 h. RT-PCR (A, B), western blot analysis (A, C), and the determination of intracellular reactive oxygen species levels (D) were then conducted. Total RNA was extracted from the cells, and RT-PCR analysis of MDR1 mRNA and GAPDH mRNA was conducted (A, B). Whole cell lysates were used for western blot analysis of P-gp and GAPDH (A, C). Intracellular reactive oxygen species levels were determined using the fluorogenic dye CDCFH (D). The photograph is typical of three independent experiments. Column graph data represent relative levels against GAPDH and are expressed as the mean ± S.D. ($n=3$). $^{*}P<0.05$, significantly different from the control. $^{\#}P<0.05$, significantly different from the DOX group.

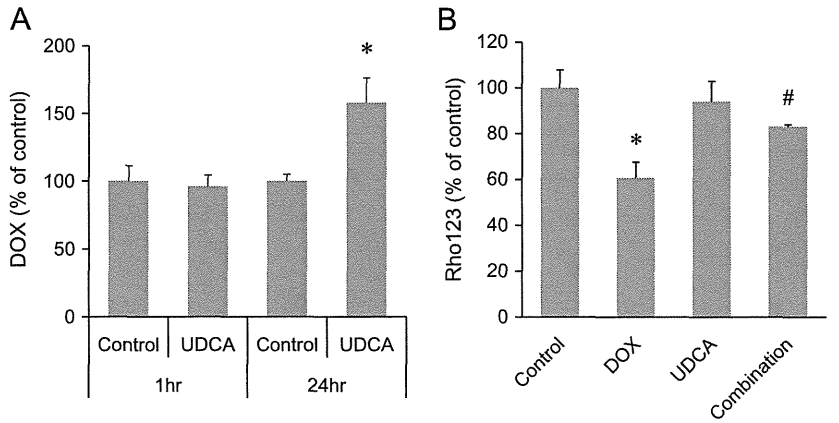

Fig. 4. Effects of UDCA on the intracellular accumulation of DOX and Rho123 in HepG2 cells. (A) HepG2 cells were pre-incubated with or without 100 μM UDCA for 1 h and then incubated with 3 μM DOX in the presence or absence of 100 μM UDCA for 1 or 24 h. Intracellular DOX levels were determined as described in the Materials and methods. (B) Cells were pre-incubated with or without 100 μM of UDCA for 1 h and then incubated with 3 μM DOX in the presence or absence of UDCA for 24 h. After changing to fresh medium, the cells were subsequently cultivated for 24 h. Cells were then incubated in fresh medium containing 3 μM Rho123 for 30 min at 37 °C. Intracellular Rho123 levels were determined as described in the Materials and methods. Fluorescence intensities of DOX and Rho123 are expressed as a relative value against cellular protein. Column graph data are expressed as the mean ± S.D. ($n=3$). $^{*}P<0.05$, significantly 1 different from the control. $^{\#}P<0.05$, significantly different from the DOX group.

DOX was previously shown to induce both an increase in intracellular reactive oxygen species content and decrease in GSH content accompanied by the activation of NF-κB (Ortiz et al., 2008). In the present study, we showed that UDCA and CDCA suppressed DOX-induced reactive oxygen species production, accompanied by the overexpression of MDR1 and P-gp, whereas DCA and LCA did not. Furthermore, we ascertained that NAC, an antioxidant, suppressed DOX-induced reactive oxygen

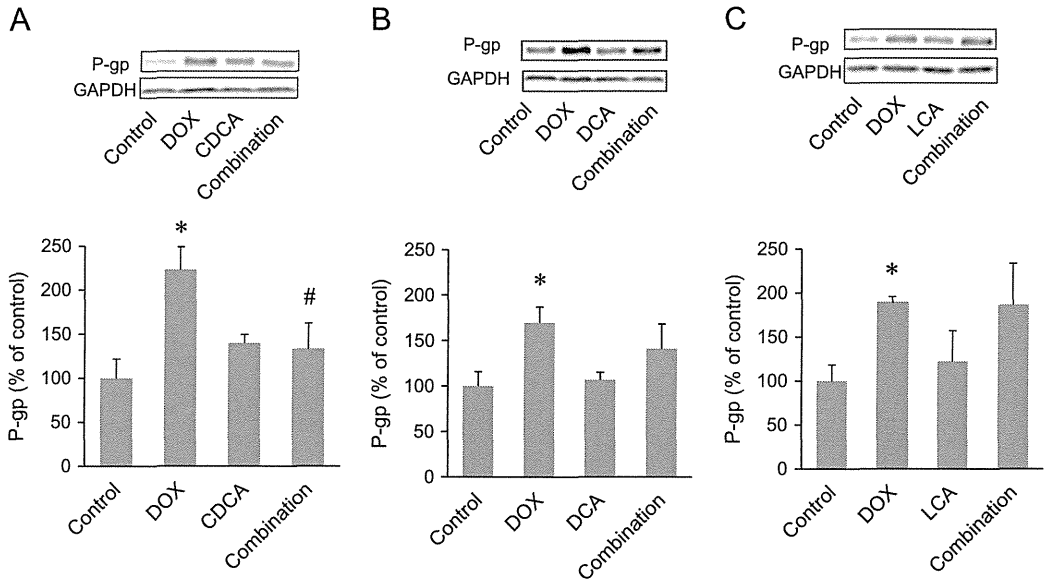

Fig. 5. Effect of CDCA, DCA, and LCA on the DOX-induced increase in P-gp levels. HepG2 cells were pre-incubated with or without 100 μM CDCA (A), 100 μM DCA (B), or 30 μM LCA (C) for 1 h and then incubated with 3 μM DOX in the presence or absence of a bile acid for 24 h. Whole cell lysates were used for western blot analysis. The photograph is typical of three independent experiments. Column graph data represent relative levels against GAPDH and are expressed as the mean ± S.D. (n=3). $^{*}P < 0.05$, significantly different from the control. $^{\#}P < 0.05$, significantly different from the DOX group.

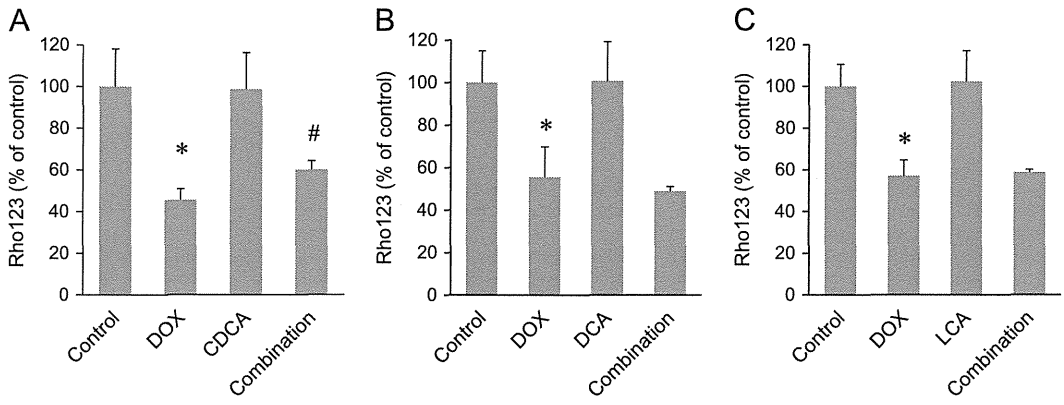

Fig. 6. Effects of CDCA, DCA, and LCA on the uptake of Rho123 in cells. HepG2 cells were pre-incubated with or without 100 μM CDCA (A), 100 μM DCA (B), or 30 μM LCA (C) for 1 h and then incubated with 3 μM DOX in the presence or absence of a bile acid for 24 h. After the cells were further cultivated in fresh medium for 24 h, they were incubated in fresh medium containing 3 μM Rho123 for 30 min at 37 °C. Fluorescence intensity was evaluated as a relative value against intracellular protein. Column graph data are expressed as the mean ± S.D. (n=3–6). $^{*}P < 0.05$, significantly different from the control. $^{\#}P < 0.05$, significantly different from the DOX group.

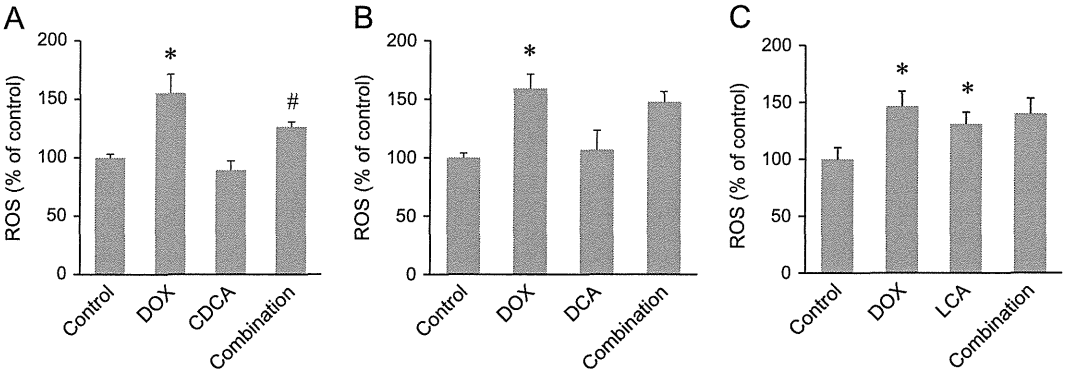

Fig. 7. Effects of CDCA, DCA, and LCA on reactive oxygen species levels in cells. After the pre-incubation of HepG2 cells with or without 100 μM CDCA (A), 100 μM DCA (B), or 30 μM LCA (C), cells were incubated with or without 3 μM DOX for 3 h in the presence or absence of bile acids. Intracellular reactive oxygen species levels were determined using the fluorogenic dye CDCFH. Fluorescence intensity was evaluated as a relative value against intracellular protein. Column graph data are expressed as the mean ± S.D. (n=3). $^{*}P < 0.05$, significantly different from the control. $^{\#}P < 0.05$, significantly different from the DOX group.